

---

Research Article: New Research | Disorders of the Nervous System

## Seizure prediction in genetic rat models of absence epilepsy: improved performance through multiple-site cortico-thalamic recordings combined with machine learning

<https://doi.org/10.1523/ENEURO.0160-21.2021>

**Cite as:** eNeuro 2021; 10.1523/ENEURO.0160-21.2021

Received: 13 April 2021

Revised: 26 October 2021

Accepted: 2 November 2021

---

*This Early Release article has been peer-reviewed and accepted, but has not been through the composition and copyediting processes. The final version may differ slightly in style or formatting and will contain links to any extended data.*

**Alerts:** Sign up at [www.eneuro.org/alerts](http://www.eneuro.org/alerts) to receive customized email alerts when the fully formatted version of this article is published.

Copyright © 2021 Budde et al.

This is an open-access article distributed under the terms of the Creative Commons Attribution 4.0 International license, which permits unrestricted use, distribution and reproduction in any medium provided that the original work is properly attributed.

1 **1. Manuscript title:** Seizure prediction in genetic rat models of absence epilepsy: improved  
2 performance through multiple-site cortico-thalamic recordings combined with machine  
3 learning

4  
5 **2. Abbreviated title:** SWD prediction using an artificial neuronal network  
6

7 **3. List all Author Names and Affiliations in order as they would appear in the**  
8 **published article:**

9 Björn Budde<sup>1</sup>, Vladimir Maksimenko<sup>2</sup>, Kelvin Sarink<sup>3</sup>, Thomas Seidenbecher<sup>1</sup>, Gilles van  
10 Luijtelaar<sup>4</sup>, Tim Hahn<sup>3\*</sup>, Hans-Christian Pape<sup>1\*</sup> and Annika Lüttjohann<sup>1\*</sup>

11 <sup>1</sup>Institute of Physiology I, University of Münster, Münster, Germany

12 <sup>2</sup>Neuroscience and Cognitive Technology Lab, University of Kazan, Kazan, Russia

13 <sup>3</sup>Institute for Translational Psychiatry, University of Münster, Münster, Germany

14 <sup>4</sup>Donders Institute for Brain, Cognition and Behaviour, Radboud University Nijmegen,  
15 Nijmegen, The Netherlands

16  
17 \*Shared correspondence

18 **4. Author Contributions:** AL, HCP and GvL conceived the study; BB performed the *in vivo*  
19 experiments, with contribution by AL. BB, VM, KS, TH, AL analyzed the data; All authors  
20 discussed the results; BB, AL and HCP wrote the paper. All authors agreed to the final  
21 version of the paper.

22 **5. Correspondence:** Annika Lüttjohann, email: annika.luetjohann@ukmuenster.de, Institute  
23 of Physiology I (Neurophysiology), Westfälische Wilhelms-Universität Münster, Robert-Koch-  
24 Strasse 27a, D-48149 Münster, Germany;

25 Hans-Christian Pape, email: papechris@ukmuenster.de, Institute of Physiology I  
26 (Neurophysiology), Westfälische Wilhelms-Universität Münster, Robert-Koch-Strasse 27a, D-  
27 48149 Münster, Germany.

28 Tim Hahn, email: hahnt@wwu.de, Westfälische Wilhelms-Universität Münster, Albert-  
29 Schweitzer Campus 1 (Gebäude A9a), 48149 Münster, Germany.

30

**6. Number of Figures:** 4

**9. Number of words for Abstract:** 250

**7. Number of Tables:** 3

**10. Number of words for Significance Statement:** 118

**8. Number of Multimedia:** 0

**11. Number of words for Introduction:** 678

**12. Number of words for Discussion:** 1850

31

32

33 **13. Acknowledgements:** We would like to thank Thomas Westhoff, Tim Book and Gerard  
34 van Oijen for expert IT-support as well as Hubert Bäumer, Petra Berenbrock and Anika  
35 Böggemann for animal care. We acknowledge valuable discussion with Prof. Alexander  
36 Hramov on brain-computer interfaces and constant valuable support by 'Förderverein  
37 Epilepsieforschung an der Universität Münster e.V.'.  
38

39 **14. Conflict of Interest:** Authors report no conflict of interest

40 **15. Funding sources:** This work was supported by a grant from Innovative Medizinische  
41 Forschung (IMF) (LÜ121603) to AL, and a DAAD travel grant to VM.  
42

1

**Abstract**

Seizure prediction is the grand challenge of epileptology. Yet, effort was devoted to prediction of focal seizures, while generalized seizures were regarded as stochastic events. Long lasting LFP recordings containing several hundred generalized spike and wave discharges (SWDs), acquired at eight locations in the cortico-thalamic system of absence epileptic rats, were iteratively analyzed in all possible combinations of either two or three recording sites, by a wavelet-based algorithm, calculating the product of the wavelet-energy signaling increases in synchronicity. Sensitivity and false alarm rate of prediction were compared between various combinations and wavelet spectra of true- and false positive predictions were fed to a random forest machine learning algorithm to further differentiate between them. Wavelet analysis of intracortical and cortico-thalamic LFP traces showed a significantly smaller number of false alarms compared intrathalamic combinations, while predictions based on recordings in layer 4, 5 and 6 of the somatosensory-cortex significantly outreached all other combinations in terms of prediction sensitivity. In 24-hours out-of-sample recordings of 9 GAERS, containing diurnal fluctuations of SWD occurrence, classification of true and false positives by the trained random forest further reduced the false alarm rate by 71%, although at some tradeoff between false alarms and sensitivity of prediction, as reflected in relatively low F1-score values. Results provide support for the cortical-focus theory of absence epilepsy and allow the conclusion that SWDs are predictable to some degree. The latter paves the way for the development of closed-loop SWD prediction-prevention systems. Suggestions for a possible translation to human data are outlined.

2

**3 Significance statement**

4 Seizure prediction was declared the grand challenge of epileptology. While most effort was  
5 devoted to the prediction of focal seizures, generalized seizures were regarded as stochastic  
6 events. Results of this study demonstrate that above chance prediction of generalized spike  
7 and wave discharges (SWDs) is possible in long lasting, pseudoprospective 24 hours  
8 recordings of absence epileptic rats, by means of wavelet analysis of LFP traces acquired  
9 near the proposed cortical initiation network in S1 and further classification of true and false  
10 positive detections by a trained random forest machine learning algorithm. Moreover, as  
11 lower SWD prediction performance was achieved by analysis of LFP traces distant to S1, the  
12 study provides evidence supporting the cortical focus theory of absence epilepsy.

13

14 **Keywords:** random forest, artificial neuronal network, absence epilepsy, GAERS,  
15 somatosensory cortex, spike and wave discharges

## 16 **1. Introduction**

17 Epilepsy is a neurological disorder characterized by infrequent, short lasting periods of either  
18 local or generalized, hypersynchronous brain activity which can be recorded in the  
19 electroencephalogram. Depending on the type and nature of these seizures they either go  
20 along with a loss of behavioral control in the form of tonic or clonic convulsions and/or with a  
21 loss of consciousness. As a majority of patients diagnosed with epilepsy report the  
22 uncertainty of when a seizure attack will happen to them as one of the most disabling  
23 aspects of the disease, seizure prediction was declared the grand challenge of epileptology  
24 (Seizure Gauge Challenge 2017; 2016 Community Survey of Epilepsy Innovation Institute  
25 (Ei2) 2016; Kiral-Kornek et al. 2018).

26 At present, most effort in the development of seizure prediction algorithms has been devoted  
27 to the prediction of focal seizures, in which, a local group of abnormally discharging neurons  
28 is assumed to gradually recruit a critical mass of neurons during a putative pre-seizure state.  
29 Results on seizure prediction performance are quite variable, with multi-variable methods  
30 taking measures of synchronization between brain structures into account usually  
31 outperforming uni-variable methods (Mormann et al. 2007). Part of this variability can be  
32 attributed to methodological shortcomings, and a list of criteria based on which prediction  
33 performance should be evaluated was established to guide good scientific practice  
34 (Mormann et al. 2007). Criteria include evaluation of prediction performance based on  
35 unselected continuous data, in-sample and out-of-sample testing with unseen (pseudo)  
36 prospective data, and evaluation with rigorous and solid statistical methods like Monte Carlo  
37 surrogate statistics to test prediction performance against chance level prediction (Mormann  
38 et al. 2007; Kuhlmann et al. 2018).

39 More recently developed algorithms evaluated against these criteria, employed machine  
40 learning or deep learning approaches, and were found to achieve above chance prediction  
41 (Khan et al. 2018; Eberlein et al. 2019; Kiral-Kornek et al. 2018). Both are feature extraction  
42 methods that have been proven successful in a number of pattern recognition tasks, like  
43 image and speech recognition in medical diagnosis, genomics, translation or robotics (Walter  
44 et al. 2019; Ratner 2015; Daily et al. 2017).

45 Comparatively little effort has been devoted to the prediction of generalized seizures, as they  
46 have long been regarded as stochastic events (Lopes Da Silva et al. 2003). In two validated  
47 genetic rat model of absence epilepsy (rats of the WAG/Rij strain and Genetic Absence  
48 Epilepsy Rats from Strasbourg (GAERS)), characterized by generalized spike and wave  
49 discharges (SWDs) and a concomitant decrease in the level of consciousness (Depaulis and

50 Charpier 2018; van Luijtelaar and Zobeiri 2014), several studies reported the presence of  
51 pre-ictal changes in the corticothalamic system, that might be useful features for SWD  
52 prediction (Polack et al. 2007; Sorokin et al. 2016; Pinault et al. 2001; van Luijtelaar et al.  
53 2011; Lüttjohann and van Luijtelaar 2012). A first proof of principle for the predictability of  
54 SWDs was provided by Maksimenko et al. (2017). To achieve a measure for synchronization  
55 signaling SWD initiation, these authors calculated the product of the wavelet energy  
56 assessed in local field potential (LFP) recordings taken at three locations in the cortico-  
57 thalamic system of WAG/Rij rats. While this algorithm already reached a high sensitivity of  
58 prediction, it still suffered from a large amount of false alarms, strongly reducing the  
59 specificity of prediction.

60 The current study was designed to improve SWD prediction performance through (i) a  
61 systematic variation of the multiple recording sites of SWDs in the cortico-thalamic system  
62 and relation to SWD prediction sensitivity and false alarm rate, (ii) a thorough statistical  
63 comparison of wavelet spectra corresponding to true positive- and false positive detections,  
64 and (iii) training of a machine learning algorithm (random forest) to further differentiate  
65 between both types of detections.

66 In line with the criteria of good scientific practice mentioned above, we assessed algorithm  
67 performance in long lasting, non-selected, pseudo-prospective 24 hours recordings, taking  
68 potential diurnal variations of seizure occurrence into account (Smyk and van Luijtelaar  
69 2020), we incorporated in-sample and out-of-sample recordings (from two different genetic  
70 rat models of absence epilepsy, rats of the WAG-Rij strain and GAERS), and we statistically  
71 verified the results using surrogate statistics.

72

## 73 **2. Material and Methods**

### 74 **2.1 Animals, surgery and acquisition of LFP recordings**

75 LFP recordings of a total of 22 male WAG/Rij rats and 15 male GAERS, two well validated  
76 genetic rat models of absence epilepsy were analyzed. As both strains show several  
77 hundred spontaneously occurring SWDs per day (Depaulis and van Luijtelaar 2006), the data  
78 are potentially suited for training and evaluation of machine learning algorithms requiring a  
79 large amount of training data.

80 Recordings of 16 WAG/Rij rats were taken from a previously published data set analyzing  
81 pre-ictal network interactions in the cortico-thalamic system (Lüttjohann and van Luijtelaar  
82 2012, 2015). In these rats, LFP signals were simultaneously measured in freely moving  
83 animals in eight different brain structures within the cortico-thalamic system including the  
84 posterior thalamic nucleus (Po), the ventral-postero-medial thalamic nucleus (VPM), caudal  
85 and rostral part of reticular thalamic nucleus (cRTN and rRTN), anterior thalamic nucleus

86 (ATN) as well as layer IV, V, VI of the somatosensory cortex (S1) (coordinates are specified  
87 in Lüttjohann & van Luijtelaar, 2012). LFP signals were gathered at a constant sample rate of  
88 2048 Hz and filtered between 1 Hz high pass (HP) and 100 Hz (LP) low pass as well as by a  
89 50 Hz notch filter, over a period of at least 4 hours. A WINDAQ-recording-system was used  
90 to digitize EEG signals (DATAQ-Instruments Inc., Akron, OH, USA). Rat movement was  
91 registered via a PIR detector (RK2000DPC LuNAR PR Ceiling Mount, Rokonet RISCO  
92 Group S.A., Drogenbos, BE). In additional 6 WAG/Rij rats LFP recordings were acquired in  
93 layer Va, Vb and layer VI of the secondary motor cortex (A/P +2.7 mm, M/L +1.2 mm, d -2.5,  
94 2.6, 2.8 mm, respectively; coordinates relative to bregma). Coordinates were determined  
95 relatively to bregma and according to the stereotactic atlas of Paxinos and Watson (1998)).

96

97 LFP recordings of GAERS were acquired in the Münster lab. Animals aged 3 to 9 months,  
98 born and raised at the Institute of Physiology I, Westfälische Wilhelms-University Münster.  
99 underwent stereotactic surgery under pentobarbital anesthesia (Narcoren, 50 mg/kg;  
100 Boehringer Ingelheim Vetmedica GmbH, Ingeheim am Rhein, Germany) for the implantation  
101 of recording electrodes (stainless steel, insulated with polyamide, impedance 0.1 M $\Omega$ ;  
102 diameter 0.005 inch; Plastics One, Roanoke, USA) in the deep layer (IV, V and VI) of S1  
103 (A/P: -1.8, M/L: -3.6, d:-2.6, -2.9 -3.2). Reference and a ground electrode were placed on top  
104 of the cerebellum. Carprofen (5mg/kg) was administered to the rats 30 minutes before as  
105 well as 24 and 48 hours after surgery to ensure intra and postoperative analgesia.

106 Two weeks after surgery animals were placed in a 43x28x42 cm plexiglas recording box,  
107 equipped with bedding material, cage enrichment (Enviro-Dri) and free excess to food and  
108 water. Rats were connected to recording leads connected to a swivel commutator allowing  
109 LFP recordings in freely moving animals. LFP signals were amplified by an amplifier (TD  
110 90087, Radboud University Nijmegen, Electronic Research Group) filtered between 1 Hz  
111 (HP) and 100 Hz (LP) as well as by a 50 Hz notch filter, and digitalized with a constant  
112 sample rate of 500 Hz by WINDAQ-recording-system (DATAQ-Instruments Inc., Akron, OH,  
113 USA). In addition, a PIR (Passive Infrared Registration, RK2000DPC LuNAR PR Ceiling  
114 Mount, Rokonet RISCO Group S.A., Drogenbos, BE) registered rat movements. GAERS  
115 were recorded for a total of 24 hours.

116 All experimental procedures were carried out according to the guidelines and regulations of  
117 the council of the European Union (Directive 2010/63/EU) and were approved by local  
118 authorities.

119

## 120 **2.2 Data processing and statistics**

121 **2.2.1. Wavelet-based SWD prediction by the Maksimenko et al (2017) algorithm –**  
122 **comparison between combinations of recording sites in the cortico-thalamic system.**

123 In an attempt to determine the optimal recording sites for SWD prediction and to gain  
124 additional insight into network interactions in the cortico-thalamic system in relation to the  
125 generation of SWD, we assessed SWD prediction performance in all possible combinations  
126 of two and three different recording sites in the cortico-thalamic system (Table I) using the  
127 algorithm previously published by Maksimenko et al (2017).

128

129 For SWD prediction, the Maksimenko et al (2017) algorithm determines in each LFP trace,  
130 the mean wavelet energy within a time window of 500 ms shifting along the complete LFP  
131 trace sample by sample. In each trace (i) and at each time step (t), the wavelet energy (W)  
132 within the frequency range of 5-10 Hz corresponding to the precursor ( $W_{(5-10 \text{ Hz})}(t)$ ) is  
133 calculated using wavelet transformation with a modified Morlet mother function (Maksimenko  
134 et al. 2017; van Luijtelaaar et al. 2016). This energy obtained in each trace is multiplied to  
135 determine the occurrence of cortico-thalamic synchronization at each moment in time ( $W_{(5-10 \text{ Hz})}(t) = W1_{(5-10 \text{ Hz})}(t) \times W2_{(5-10 \text{ Hz})}(t) \times W3_{(5-10 \text{ Hz})}(t)$ ). Moreover, wavelet energy is calculated and  
136 multiplied in each channel for a frequency range of 3-5 Hz in accordance to the light slow  
137 wave sleep ( $W_{(3-5 \text{ Hz})}(t) = W1_{(3-5 \text{ Hz})}(t) \times W2_{(3-5 \text{ Hz})}(t) \times W3_{(3-5 \text{ Hz})}(t)$ ) and within a frequency  
138 range of 7-20 Hz representing sleep spindles ( $W_{(7-20 \text{ Hz})}(t) = W1_{(7-20 \text{ Hz})}(t) \times W2_{(7-20 \text{ Hz})}(t) \times W3_{(7-20 \text{ Hz})}(t)$ ) (Figure 4A).

141 Decision on whether a SWD precursor is present is based on three criteria:

- 142 1. Energy of  $W_{(5-10 \text{ Hz})}(t)$  needs to exceed an individualized specific threshold.
- 143 2. Energy of  $W_{(5-10 \text{ Hz})}(t)$  must exceed energy of  $W_{(3-5 \text{ Hz})}(t)$
- 144 3. Energy of  $W_{(5-10 \text{ Hz})}(t)$  must exceed energy of  $W_{(7-20 \text{ Hz})}(t)$

145

146 For determination of optimal recording sites for SWD prediction, LFP recordings (duration 4  
147 hours), simultaneously obtained within the cortico-thalamic system in GAERS and WAG/Rij  
148 rats, were fed into the wavelet-based SWD prediction algorithm of Maksimenko et al. (2017),  
149 testing data from the various recordings sites in all possible combinations (Table I). For  
150 WAG/Rij rats, a total number of 57 combinations composed of LFP recordings from three  
151 recording sites and 28 combinations, composed of LFP recordings from two recording sites  
152 (see Table I), were presented to the algorithm. For GAERS, data from three recording sites  
153 in layers IV, V and VI of S1 were used. Each combination of recording sites can be found in  
154 Table I; 'C','T','M' globally refers to recording sites in somatosensory cortex (S1), thalamus  
155 and secondary motor cortex, respectively.

156

157 Since SWD prediction quality depends on the above mentioned individualized threshold,  
158 SWD prediction performance of each recording site combination was determined for a total

159 of 14 fixed threshold values ranging from 0.1 to 0.75 for all combinations of three recording  
160 sites, and a total of 16 fixed threshold values ranging from 0.005 to 0.04 for all combinations  
161 composed of two recording sites. Of note, the difference in magnitude in the threshold values  
162 for two and three recording sites is attributed to the fact that detection relies on the product of  
163 either two or three wavelet energy values (see above). For prediction based on two versus  
164 three recording sites, the outer threshold levels (minimum and maximum) correspond to  
165 saturated levels of either sensitivity or false alarm rates for all tested combinations.

166

167 Detections of the algorithm occurring within a 1s pre-ictal period before SWD onset were  
168 regarded as true positives, while detections at interictal timepoints were regarded as false  
169 positives. SWD onset was determined according to the criteria outlined by van Luijtelaar &  
170 Coenen (1986), taking the peak of the first spike of twice the amplitude of the background  
171 EEG as a reference to mark the onset of the SWD (Figure 1). In case of differences in spike  
172 timing between recording sites, notably occurring in the range of milliseconds (Lüttjohann  
173 and van Luijtelaar 2012), the peak of the first spike earliest in time was taken as SWD onset.

174

175 For each combination of recording sites, and for each of the threshold values, the sensitivity  
176 (Sensitivity = number of correctly predicted SWDs / (number of correctly predicted SWDs +  
177 number of unpredicted SWDs) × 100%) of SWD prediction as well as the false alarm rate  
178 were determined.

179 Linear regression analysis (Pearson correlation) was used to determine the degree of  
180 interdependence between the sensitivity of prediction and false alarm rate.

181 Statistical comparison of sensitivity and false alarm rate between different combinations of  
182 recording sites were performed using ANOVA with sensitivity or false alarm rate as  
183 dependent variable, combination of recording sites as between subject factor 1, number or  
184 recording sites (2, 3) as between subject factor 2, threshold as covariate 1 and false alarm  
185 rate or sensitivity as covariate 2.

186

187 To avoid multiple comparison problems all combinations of recording sites were grouped for  
188 post-hoc analyses as follows. 1: two intracortical recording sites in S1 (CC), 2: one cortical  
189 recording site in S1 and one thalamic recording site (CT), 3: two intrathalamic recording sites  
190 (TT), 4: three intracortical recording sites in S1 (CCC), 5: two cortical recording sites in S1  
191 and one thalamic recording site (CCT), 6: one cortical recording site in S1 and two thalamic  
192 recording sites (CTT), 7: three intrathalamic recording sites (TTT) and 8: three intracortical

193 recording sites in the secondary motor cortex (MCCC). Post hoc analyses included: ANOVA  
194 with sensitivity or false alarm rate as dependent variable, group of channel combinations  
195 (CC, TC, TT, CCC, CCT, CTT, TTT, MCCC) as between subject factor 1, number of  
196 recording sites (2, 3) as between subject factor 2, threshold as covariate 1 and false alarm  
197 rate or sensitivity as covariate 2.

198

199 All statistical analyses were performed using IBM SPSS version 25. Data are expressed as  
200 the arithmetic mean values  $\pm$  standard error of the mean (S.E.M.). Differences were  
201 considered statistically significant when  $p \leq 0.05$  (\*),  $p \leq 0.01$  (\*\*) and  $p \leq 0.001$  (\*\*).

202

### 203 **2.2.2 Comparison of wavelet spectra corresponding to true positive- and false positive** 204 **predictions.**

205 Irrespective of the combination of recording sites, the Maksimenko et al (2017) algorithm  
206 results in relatively high false alarm rates. Therefore, we determined pre-existing differences  
207 in spectra corresponding to either true positive- or false positive predictions. Wavelet spectra  
208 of all true positive detections, and a total number of 50 randomly selected false positive  
209 detections, as identified by the algorithm of Maksimenko et al. (2017), were calculated from  
210 LFP traces acquired in the deep layer (IV, V and VI) of S1 in GAERS and WAG/Rij rats  
211 (Figure 3). Timepoint zero indicates the timepoint of precursor detection at the end of a 500  
212 ms analysis window (ranging from -0.5 to 0), in which either the true positive precursor or the  
213 false positive was detected.

214 Average wavelet energy within different frequency bands was statistically compared between  
215 true and false detections using repeated measures ANOVA with average wavelet energy as  
216 dependent variable, type of detection (true positive, false positive) as within subjects factor 1,  
217 frequency band ( $W_{(5-10 \text{ Hz})}$ ,  $W_{(3-5 \text{ Hz})}$  and  $W_{(7-20 \text{ Hz})}$ ) as within subjects factor 2 and rat strain  
218 (GAERS, WAG/Rij rats) as between subject factor.

219

### 220 **2.2.3 Random forest machine learning algorithm for differentiation between true positive -** 221 **and false positive predictions**

222 In an attempt to further differentiate between true and false positive predictions, we trained a  
223 random forest machine learning algorithm. The wavelet energy extracted for true and false  
224 detections was fed into a random forest (Birjandtalab et al. 2017) consisting of a total of 1000  
225 decision trees (Figure 4A). Different numbers of trees were experimentally varied to  
226 investigate the effect of forest size on classification performance (Figure 4E). For each true  
227 and false positive prediction produced by the Maksimenko et al (2017) algorithm, 9 wavelet

228 energy values corresponding to the values assessed in the three frequency bands ( $W_{(5-10 \text{ Hz})}$ ,  
229  $W_{(3-5 \text{ Hz})}$  and  $W_{(7-20 \text{ Hz})}$ ) at three different recording sites, were presented to the algorithm to  
230 extract features for classification (Figure 4A). Majority voting of the different trees in the  
231 random forest yielded final classification (Figure 4A).

232

233 Training of the random forest was performed with spectra obtained in 70% of all recorded  
234 data in 6 WAG/Rij rats and 6 GAERS, and classification performance was evaluated on the  
235 remaining 30% of unseen data of the same rats (i.e. in-sample testing). As epileptic seizures  
236 or pre-ictal events are underrepresented compared to the vast number of inter-ictal  
237 fragments or false positive predictions, a random undersampling approach was taken in a  
238 first step in order to create a balanced training set and thereby ensure balanced learning  
239 (Kubat et al. 1997). All true positive detections were fed into the algorithm, matched by an  
240 equal number of randomly selected false positive detections. In this way a total of 100  
241 random forest were trained. Of note, each random forest was fed with a different set of false  
242 positive detections. Obtained results correspond to the performance of a single trained  
243 random forest, which was found to reach an average performance of these 100 trained trees.

244

245 In order to allow an unbiased comparison of classification performance of the random forest  
246 between different combinations of recording sites, we adjusted the detection threshold of the  
247 Maksimenko et al algorithm (2017) for each combination to reach a 60% sensitivity of SWD  
248 prediction for the extraction of the time points and wavelet features for training and  
249 evaluation of classification.

250

251 To assess the classification performance of the random forest the balanced accuracy of  
252 classification was calculated as  $(\text{sensitivity of classification} + \text{specificity of classification}) / 2$ ,  
253 with  $\text{specificity} = (\text{number of false positives predicted as false positives} / (\text{number of false}$   
254  $\text{positives predicted as false positives} + \text{number of false positives predicted as true positives}))$   
255  $\times 100\%$  and  $\text{sensitivity} = (\text{number of true positives predicted as true positives} / (\text{number of}$   
256  $\text{true positives predicted as true positives} + \text{number of true positives predicted as false}$   
257  $\text{positives})) \times 100\%$ . Moreover an F1-score defined as  $F1 = 2 \times ((\text{precision} \times \text{sensitivity}) /$   
258  $(\text{precision} + \text{sensitivity})) \times 100\%$  was calculated, where  $\text{precision} = (\text{number of true}$   
259  $\text{positives predicted as true positives} / (\text{number of true positives predicted as true positives} +$   
260  $\text{number of false positives predicted as true positives})) \times 100\%$ .

261 Classification performance of the random forest was compared with ANOVA between the  
262 different groups of recording sites in WAG/Rij rats: 1. Recordings in layers V and VI of S1,  
263 referred to as “CC” (n=145); 2. Recordings in layers IV, V and VI of S1, referred to as “CCC”  
264 (n=161); 3. Recordings in layers IV, VI of S1 and VPM, referred to as “CCT” (n=161); 4.

265 Recordings in layer VI of S1, VPM and RTN, referred to as “CTT” (n=161); 5. Recordings in  
266 VPM, cRTN and Po, referred to as “TTT” (n=145), 6. recordings in layer Va, Vb and VI of  
267 secondary motor cortex, referred to as “MCCC” (n=161). In addition, classification  
268 performance was assessed in recordings from layers IV, V and VI of S1 in GAERS, referred  
269 to as “GCCC” (n=145, n=161, n=1844) and compared to results achieved in WAG/Rij rats  
270 using ANOVA. Furthermore, classification performance of each group was evaluated against  
271 chance level using surrogate statistics (see below).

272

#### 273 **2.2.4 Probing the random forest machine learning algorithm for maximal SWD prediction** 274 **performance**

275 Next, the random forest machine learning combined with the Maximenko et al. (2017)  
276 algorithm were probed for maximal prediction performance of SWD. Wavelet features for true  
277 and false predictions were extracted in LFP recordings obtained in the deep layers (IV, V and  
278 VI) of S1 of 6 GAERS at a threshold value reaching a 90% sensitivity for SWD prediction,  
279 and were used for training and in-sample testing as described above. Moreover,  
280 performance of random-forests trained in this approach were assessed in unseen 24 hours  
281 recordings from a separate group of 9 GAERS rats (out-of-sample testing).

282

283 For in-sample testing and out-of sample testing, performance was statistically evaluated  
284 against chance level prediction using surrogate statistics. To this end, training data of true  
285 and false detections were randomly assigned to the two classes (total of 1000  
286 randomizations), and for each randomization the average balanced accuracy achieved in the  
287 unseen data was determined and displayed in a histogram. In case the achieved balanced  
288 accuracy computed for the random forest trained with the real (i.e. non-randomized) training  
289 data was positioned above the 95th quantile of the histogram, algorithm performance was  
290 regarded as significant above chance level.

291

292 Lastly, as classification performance of the random forest was found to be reduced in the  
293 out-of-sample testing, likely resulting from an insufficient amount of false positive predictions  
294 presented to the algorithm during training, a separate set of random forests (n=100) was  
295 trained in a (moderate) oversampling approach. A multiple (4) of all true positive predictions  
296 and a matched number of randomly selected false positive predictions, derived in LFP  
297 recordings of the deep layer (IV, V and VI) of S1 in 6 GAERS at a threshold value of 90%,  
298 were used to train the random forests. Determination of an appropriate oversampling factor  
299 was performed by comparison of classification performances achieved at different  
300 oversampling factors, ranging between 2 to 7. Higher rates of oversampling were omitted to

301 avoid overtraining. As for the under-sampling approach, classification performance was  
302 assessed in unseen 24 hours recordings from a separate group of 9 GAERS rats (out-of-  
303 sample testing) and tested against chance level using surrogate statistics (see above).

304

305 Performance presented in the results corresponds to the performance of a single trained  
306 random forest, reaching an average performance of these 100 trained trees.

307

### 308 **2.3 Histology**

309 At the end of the recordings, a direct current (9 V, 25  $\mu$ A, 2 s duration) was pathed though  
310 each electrode to create an electrolytic lesion at the location of the tip of the electrode.  
311 Animals were killed with an intraperitoneal injection of pentobarbital (Narcoren, 150 mg/kg;  
312 Merial GmbH, Münster, Germany). The brain was quickly removed and placed in a 4%  
313 paraformaldehyde (PFA) solution for at least 24 h. Brains were fixated in a 30% sucrose  
314 solution and cut into 60  $\mu$ m slices with the aid of a microtome. Slices were mounted on  
315 microscope slides, stained with cresyl violet, and inspected under a light-microscope (dnt,  
316 DigiMicro Profi) for identification of the microlesions. Recording sites were extrapolated from  
317 the center of the lesion relative to cortical depth and neighboring cortical layers. Only  
318 recordings from verified recording positions were included in the analysis.

319

### 320 **2.4 Code Accessibility**

321 The random forest algorithm was programmed in Python and requires previous installation of  
322 Python for execution. The code of the random forest algorithm is available as Extended Data.

323

## 324 **3. Results**

### 325 **3.1 Electrophysiological characteristics of SWDs in GAERS and WAG/Rij rats**

326 Exemplary LFP recordings of GAERS and WAG/Rij rats are displayed in Figure 1. LFP  
327 signals of GAERS, recorded for 24 hours, displayed frequent (average of 17 per hour) SWDs  
328 of 10 to 30 seconds duration at a main frequency of 5–7 Hz. Occurrence of SWDs showed  
329 the well documented diurnal variation with highest rates of occurrence at the beginning of the  
330 dark phase and lowest rates of occurrence at beginning of the light phase (Smyk and van  
331 Lujtelaar 2020). LFP signals in WAG/Rij rats were acquired during four hours of the dark  
332 phase. WAG/Rij rats showed on average 10 SWDs per hour, with a mean duration of 7 s and  
333 a slightly higher internal frequency of 8–10 Hz. Spikes in thalamus typically possessed a  
334 smaller amplitude (500 vs 700  $\mu$ V) and broader form, with a reversed polarity as compared to  
335 those in cortex. All differences of SWD morphology between strains (i.e. different internal

336 frequency) and recording sites (i.e. amplitude, polarity and sharpness of spike) are in  
337 accordance with previously published data (Sitnikova and van Luijtelaar 2007; Lüttjohann  
338 and van Luijtelaar 2012; Akman et al. 2010).

339

340 - place figure 1 about here –

341 - place table I about here –

342

343

### 344 **3.2 Influence of cortico-thalamic recording sites on SWD prediction performance**

345 In a first set of experiments, we sought to identify the influence of LFP recording sites on  
346 SWD prediction performance. LFP recordings were simultaneously obtained at multiple sites  
347 in the cortico-thalamic system of WAG/Rij rats, specifically in the deep layers (IV, V and VI)  
348 of the somatosensory cortex (S1), secondary motor cortex, and thalamic nuclei VPM, PO,  
349 ATN, rostral and caudal RTN.

350 Recordings from either two or three sites in all possible combinations (yielding a total of 85  
351 combinations) were fed into the wavelet-based algorithm (Maksimenko et al. 2017).  
352 Sensitivity and false alarm rate of the algorithm were compared in these 85 combinations  
353 (Table I). For post-hoc analysis combinations were grouped as either 'CC' (two intracortical  
354 recording sites in S1), 'CT' (one cortical recording site in S1 and one thalamic recording site),  
355 'TT' (two intrathalamic recording sites), 'CCC' (three intracortical recording sites in S1), 'CCT'  
356 (two cortical recording sites in S1 and one thalamic recording site), 'CTT' (one cortical  
357 recording site in S1 and two thalamic recording sites), 'TTT' (three intrathalamic recording  
358 sites) or 'MCCC' (three intracortical recording sites in the secondary motor cortex),  
359 respectively. Moreover, SWD prediction performance of each combination of recording sites  
360 was determined at multiple threshold values employed for precursor detection. As ANOVA  
361 revealed a significant influence of threshold on both sensitivity of prediction  
362 ( $F(1,10980)=3995$ ,  $p<0.001$ ,  $R^2=0.26$ ) (the higher the threshold, the lower the sensitivity) and  
363 false alarm rate ( $F(1,10980)=10.7$ ,  $p<0.05$ ,  $R^2=0.1$ ) (the higher the threshold, the lower the  
364 false alarm rate), threshold was taken as a covariate factor into statistical analysis in order to  
365 allow comparison of prediction performance between different combinations of recording  
366 sites irrespective of any possible threshold effects.

367

368 ANOVA revealed significant differences in both the achieved sensitivity of prediction as well  
369 as the produced false alarm rate between the different combinations of recording sites  
370 ( $F_{\text{sensitivity}}(84, 10980) = 13.47$ ,  $p<0.001$ ,  $R^2=0.37$ ;  $F_{\text{nFF}}(84, 10980) = 2.47$ ,  $p<0.001$ ,  $R^2=0.1$ )  
371 (Figure 2, Table I).

372

- place figure 2 about here -

373 On average, predictions based on three recording sites reached significantly higher  
374 sensitivities (Figure 2A, Table I) and lower false alarm rates (Figure 2C, Table I) as  
375 compared to predictions based on two recording sites ( $F_{\text{sensitivity}}(1, 10980) = 935.7, p < 0.001,$   
376  $R^2 = 0.07; F_{\text{nFP}}(1, 10980) = 116.3, p < 0.001, R^2 = 0.02$ ).

377 Regarding the false alarm rate (Figure 2C, Table I) predictions based on three intracortical  
378 recordings in S1 (CCC) and predictions based on cortico-thalamic recording sites (CCT and  
379 CTT) showed a significantly smaller number of false alarms compared to predictions based  
380 on three intrathalamic recordings (TTT) (all  $p < 0.001$ ) (average false alarm rate of CCC =  
381  $85.2 \pm 10.6$ , CTT =  $94.7 \pm 3.0$ , CCT =  $70.6 \pm 3.5$  and TTT =  $110.2 \pm 5.4$ ). Predictions based on  
382 three intracortical recordings acquired in the secondary motor cortex (MCCC), on the other  
383 hand, resulted in significantly more false alarms (average false alarm rate MCCC =  $129.8 \pm$   
384  $17.9$ ) as compared to predictions based on CCC, CCT and CTT combinations (all  $p < 0.05$ ).  
385 Highest false alarm rates with an average of  $221.1 \pm 6.2$  were found for predictions based on  
386 two intracortical recordings acquired in S1 (all  $p < 0.001$ ).

387 Regarding the sensitivity of SWD prediction, predictions based on recordings in layer IV, V,  
388 and VI of S1 significantly outreached all other combinations with an average sensitivity of  
389  $61.7 \pm 1.5\%$  (all  $p < 0.001$ ) (Figure 2A, Table I).

390 Among the remaining combinations with three recording sites, MCCC, TTT and CTT showed  
391 significantly lower sensitivities compared to predictions based on two recording sites in S1  
392 combined with one thalamic site (CCT) (all  $p < 0.001$ ) (Figure 2A, B, Table I). Lowest  
393 sensitivity was reached for predictions on two thalamic recordings (average sensitivity TT =  
394  $13.7 \pm 0.8\%$ ), while predictions based on two cortical recording sites in S1 reached a medium  
395 sensitivity of  $33.0 \pm 0.9\%$  (Figure 2A, B, Table I).

396

397 To estimate the degree of interdependence between achieved sensitivity of SWD prediction  
398 and resulting false alarm rate regression analysis was performed. Analysis revealed a  
399 significant negative correlation between both indicators of SWD prediction performance ( $r = -$   
400  $0.716; p < 0.001$ ) (Figure 2E), indicating that a higher SWD prediction sensitivity, achieved for  
401 a given combination of recording sites, does not occur at the trade-off of a high false alarm  
402 rate. The same clusters as described above could be identified in the regression pattern  
403 including higher false alarm rates and lower sensitivities for predictions on two recording  
404 sides within the cortico-thalamic system, highest false alarm rate and medium sensitivity for  
405 predictions based of two intracortical recordings in S1, medium sensitivity and medium false  
406 alarm rate for predictions based on three intracortical recordings in M2 and highest sensitivity  
407 with a low false alarm rate for prediction based on three intracortical recordings in S1 (Figure

408 2). Of note, irrespective of recording site combination, algorithm performance remained at a  
409 low level including only moderate sensitivities of SWD prediction and high false alarm rates.

410

### 411 **3.3 Out-of-sample testing: Comparison between rat strains**

412 Both, GAERS and WAG/Rij rats are well validated genetic rat models of absence epilepsy  
413 sharing genetic, physiological and behavioral characteristics (Depaulis and van Luijtelaar  
414 2006), although slight, but significant differences in electrophysiological parameters of SWDs  
415 have been reported (Akman et al. 2010). Therefore, we evaluated the prediction performance  
416 of the Maksimenko et al. (2017) algorithm also in GAERS. Prediction performance was  
417 assessed in 4 hours lasting LFP recordings, obtained in layers IV, V and VI of S1 in GAERS  
418 and WAG/Rij rats, and, was compared between the two strains. Significant differences  
419 between rat strains were revealed for the produced false alarm rate, with significantly more  
420 false alarms in WAG/Rij rats compared to GAERS ( $p < 0.001$ ) (Figure 3B). On the other hand,  
421 no significant differences were seen between GAERS and WAG/Rij rats for the sensitivity of  
422 prediction ( $p > 0.05$ ) (Figure 3A).

423

### 424 **3.4 Comparison of true and false positive detections**

425 Irrespective of the combination of recording sites, the Maksimenko et al (2017) algorithm  
426 resulted in relatively high false alarm rates. Therefore, we determined pre-existing  
427 differences in spectra corresponding to either true positive- or false positive predictions in a  
428 next experimental step.

429 Figure 3 D and E depict exemplary spectrograms of true and false positive SWD predictions,  
430 respectively. Time point -0.5 to 0 features the analysis window (window size 500 ms) in  
431 which either the true positive precursor or the false positive was detected. The onset of the  
432 SWD is depicted at time point 0.4 seconds on the x-axis (Figure 3C,D). At this point a strong  
433 increase in the product of the wavelet energy can be noted in the main frequency band of the  
434 SWD (i.e. 5-10 Hz). On average, precursor activity around 900 to 300 ms before SWD onset.

435

436 - place figure 3 about here -

437

438 Next, the product of wavelet energy, assessed in the frequency bands  $W_{(5-10 \text{ Hz})}$ ,  $W_{(3-5 \text{ Hz})}$  and  
439  $W_{(7-20 \text{ Hz})}$  (Maksimenko et al. 2017), was statistically compared between true and false  
440 positives across the two rat strains. Data revealed significant differences between true and  
441 false positives in the frequency bands  $W_{(5-10 \text{ Hz})}$  and  $W_{(3-5 \text{ Hz})}$ . False positives possessed a  
442 higher wavelet-energy product as compared to true-positives (all  $p < 0.05$ ). For both frequency

443 bands, this difference was significantly more pronounced in GAERS compared to WAG/Rij  
444 rats ( $F(2,28)=7.3$ ,  $p<0.05$ ,  $R^2=0.3$ ) (Figure 3 F,G).

445

### 446 **3.5 A random forest machine learning algorithm for improvement of SWD prediction**

447 Since significant differences in the wavelet spectra of true and false positives were revealed,  
448 a random forest machine learning algorithm was trained to differentiate between true positive  
449 and false positive detections. In a first step, a random undersampling approach was used to  
450 create a training data set. Here, true positives detected in 70% of recordings from 6 WAG/Rij  
451 or 6 GAERS rats and an equal amount of randomly selected false positives derived from  
452 70% of recordings in the same rats were used as training data. For in-sample performance  
453 evaluation, the algorithm was confronted with the remaining 30% of unseen data (see  
454 methods section for more details). As in the paragraphs above, classification performance of  
455 the random forest was compared between different combinations of recording sites in  
456 WAG/Rij rats and between rat strains (Figure 4).

457

- place figure 4 about here -

458 In WAG/Rij rats, classification performance of the random forest was significantly above  
459 chance level for all combinations of recording sites (average balanced accuracy CCC =  
460 71.5%, CCT = 66,7%, CTT = 63,2%, CC = 62,5%) (all  $p<0.05$ ) except for spectra derived  
461 from three intrathalamic recording sites (average balanced accuracy TTT = 56,2%) ( $p>0.05$ )  
462 and spectra derived from recordings in layer Va, Vb and VI of the secondary motor cortex  
463 (average balanced accuracy MCCC = 49,9%) ( $p>0.05$ ) (Figure 4B). Highest classification  
464 accuracies were derived from three intracortical recordings acquired in S1, as was seen  
465 using the Maksimenko algorithm above (all  $p<0.05$ ). Classification accuracies for spectra  
466 derived from three intracortical recordings in S1 from GAERS were significantly higher  
467 (balanced accuracy GCCC1841 = 78,8%) compared to those in WAG/Rij rats (balanced  
468 accuracy GCCC1841 = 78,8% vs. balanced accuracy CCC = 71,5%,  $p<0.05$ ). Of note, this  
469 strain difference could not be attributed to the difference in the amount of training samples  
470 (i.e. 1841 derived from 70% of the six 24 hours recordings of GAERS vs 161 derived from  
471 70% of the six 4 hours recordings of WAG/Rij rats), as a reduction of the training data in  
472 GAERS still resulted in higher classification accuracies than in WAG/Rij rats (balanced  
473 GCCC161 = 73.6% vs balanced accuracy CCC = 71,5%,  $p<0.05$ ) (Figure 4B).

474 In order to evaluate if classification accuracy of the random forest depends on the level of  
475 sensitivity achieved by the Maksimenko algorithm, classification performance in GAERS and  
476 WAG/Rij rats achieved at sensitivities of 60% and 90% were compared for spectra derived in  
477 recordings of layer IV, V and VI in S1. In both strains, a small but significant reduction in

478 classification accuracy was noted for spectra derived at a 90% sensitivity as compared to  
479 spectra derived at a 60% sensitivity (balanced accuracy CCC = 71.5% vs CCC90% = 63.3%  
480  $p < 0.001$ ; GCCC1841 = 78.8% vs GCCC90% = 73.1%  $p < 0.001$ ). Of note, classification  
481 accuracies for spectra derived at a sensitivity of 90% significantly exceeded chance level  
482 classification as indicated by surrogate statistics (both  $p < 0.01$ ) (Figure 4B). Moreover,  
483 accuracies gradually increased towards a maximum at around 16 trees (Figure 4E).

484 For out-of-sample evaluation, the random forest trained on spectra derived from three  
485 intracortical recordings in S1 of GAERS at a sensitivity of 90% was confronted to spectra  
486 derived from 24 hours recordings in a separate group of GAERS ( $n=9$ ).

487 Table II depicts the achieved balanced accuracies of each rat as well as the average  
488 confusion matrix, specifying the relative percentage of true positives that had been classified  
489 as such (lower right corner), true positives that had been incorrectly classified as false  
490 positives (lower left corner), false positives correctly classified as such (upper left corner),  
491 and false positives incorrectly classified as true positives (upper right corner). Classification  
492 performance drastically dropped and above chance classification tested by permutation  
493 statistics was only achieved in a single rat (i.e. rat 5, balanced accuracy 59,62%,  $p < 0.05$ ).

494

495

- place Table II about here -

496 As the low performance of the random forest in the out-of-sample evaluation might be  
497 attributed to random undersampling (i.e. the algorithm was trained with a training set which  
498 does not adequately represent the full spectrum/variance of the false positive spectra), we  
499 next evaluated the performance of an random forest, which was trained in a (moderate)  
500 oversampling approach. In this approach the random forest was trained with four times all  
501 true positive detections and a matched number of randomly selected false positive  
502 detections, derived in three intracortical recordings in S1 of GAERS at a sensitivity of 90%  
503 (see methods for details). Again, for out-of-sample evaluation, the trained random forest was  
504 confronted to spectra derived from 24 hours recordings in a separate group of nine GAERS.

505 Table III depicts the achieved balanced accuracies of each individual rat as well as the  
506 average confusion matrix.

507

- place Table III about here -

508 Taking this (moderate) oversampling approach, the achieved balanced accuracies of the  
509 random forest significantly increased ( $F(1,8)=26.8$ ,  $p < 0.001$ ,  $R^2=0.7$ ), and above chance  
510 classification could be achieved in all subjects except one (permutation statistics, all but one  
511  $p < 0.05$ ) (Table III).

512 Classification of the random forest trained with the (moderate) oversampling approach  
513 resulted in a strong reduction in the false alarm rate. While the Maximenko et al (2017)

514 algorithm alone produced an average number of 9388 false alarms within the 24 hours,  
515 sorting of the random forest reduced the false alarm rate by  $71,4 \pm 2.6\%$ . Reduction of the  
516 false alarm rate, however, occurred at some tradeoff between false alarm rate and  
517 sensitivity. Here, Maksimenko et al (2017) on average correctly predicted 368 out of 409  
518 SWD, while 40 SWD were not detected (corresponding to a sensitivity of 90%). Following  
519 sorting by the random forest, an average of 200 out of 409 SWD were correctly predicted  
520 (corresponding to a sensitivity of 49%). It has to be mentioned, however, that rather large  
521 inter-individual differences occurred in prediction performance using the combined  
522 “Maksimenko et al + random forest” algorithm. Highest performance was seen in a rat in  
523 which 349 out of 520 SWD were correctly predicted (corresponding to a sensitivity of 67%).  
524

#### 525 **4. Discussion**

526 The current study was designed to improve the prediction of SWDs, a type of generalized  
527 seizures seen in several forms of absence epilepsy (Panayiotopoulos et al. 1992). While  
528 these types of seizures have long been regarded as stochastic events (Lopes Da Silva et al.  
529 2003), a recent study by Maksimenko et al. (2017) aimed at prediction of SWDs through the  
530 use of a dedicated algorithm, which calculates the product of the wavelet energy in LFP  
531 recordings taken at three locations in the cortico-thalamic system of absence epileptic rats. A  
532 drawback was that this algorithm suffered from a large amount of false positive detections.  
533 Therefore, the current study was designed to improve prediction performance, as quantified  
534 by sensitivity, specificity and balanced accuracy of prediction. The rationale was to  
535 systematically vary the sites of simultaneous recordings in the cortico-thalamic system,  
536 including somatosensory and motor cortices, rostral and caudal RTN, specific (VPM) and  
537 higher order thalamic nuclei (PO, ATN), in view of their distinct role in initiation, spread and  
538 synchronization of SWDs (Depaulis et al. 2016; Lüttjohann and van Luijtelaaar 2015; Crunelli  
539 et al. 2020). Results were iteratively analyzed, in that all possible combinations of the 2-3  
540 simultaneous recording sites were compared by using the algorithm of Maksimenko et al.,  
541 (2017). Moreover, a thorough comparison of wavelet spectra corresponding to true and false  
542 positive detections was performed and a random forest machine learning algorithm was  
543 trained to further differentiate between true and false positives. Algorithm performance was  
544 evaluated according to the guidelines of good scientific practice (Mormann et al. 2007;  
545 Kuhlmann et al. 2018) (long lasting, non-selected, pseudo-prospective 24 hours recordings  
546 with both in-sample and out-of-sample periods, evaluation against chance level prediction  
547 using surrogate statistics), and it was found to reduce the false alarm rate by on average  
548 71.4%

549  
550

551 **4.1 Highest SWD prediction performance is achieved with analysis of LFP signals in**  
552 **the close proximity of the seizure initiation network in S1**

553 Comparison of a total of 85 combinations of recording sites within the cortico-thalamic  
554 system (Table I), revealed that prediction performance was best when based on analysis of  
555 the wavelet energy of recordings obtained by three recording electrodes within the deep  
556 layers of the somatosensory cortex. SWDs are well known to be generated in the cortico-  
557 thalamic system. While the exact interactions between cortex and thalamus are still a matter  
558 of debate, accumulating evidence indicates that SWDs originate from a local intracortical  
559 initiation network in the peri-oral region of the somatosensory cortex (Crunelli et al. 2020;  
560 Jarre et al. 2017; Meeren et al. 2002). In GAERS, the crucial role of layer V and VI of S1 has  
561 been highlighted, as these layers were found to contain abnormally (i.e. hyperactively)  
562 discharging neurons, which drove neuronal activity in other cortical layers as well as thalamic  
563 activity (Lüttjohann and Pape 2019; Polack et al. 2007). These epileptogenic neurons  
564 display activity patterns strikingly similar to the precursor oscillations detected by the  
565 algorithm in the present study, including an increase in activity within up to two seconds  
566 before SWD onset and a firing frequency of around 10 Hz (Polack et al. 2007). Highest  
567 sensitivity of prediction was achieved by the Maksimenko et al (2017) algorithm based on  
568 analysis of wavelet energy in the deep layers of S1 (IV, V, VI), which significantly outreached  
569 all other cortico-thalamic- and intrathalamic combinations of recording sites (Figure 2A).  
570 Moreover, further classification of true and false positive detections by a trained random  
571 forest also reached highest, above chance balanced accuracies for spectra derived in the  
572 deep layers of S1, while classification based on intrathalamic-spectra failed to achieve above  
573 chance balanced accuracies (Figure 4B). These data are in line with the concept of a local  
574 intracortical initiation network in S1 (Meeren et al. 2002; Polack et al. 2007).

575 Interestingly, prediction performance of the Maksimenko et al. (2017) algorithm significantly  
576 dropped upon reducing the number of simultaneous recordings sites in the deep  
577 somatosensory layers from three to two (Figure 2), further demonstrating the importance of  
578 local intracortical synchronization in S1 for SWD generation. The concurrent increase in the  
579 false alarm rate might indicate a lack of information concerning the generation of other  
580 synchronized oscillations, which might be transmitted to the deep cortical layers by other  
581 subcortical structures (Sitnikova et al. 2009; Depauls et al. 1990).

582 The sensitivity of SWD prediction based on three simultaneous recordings in S1 also  
583 outreached the one achieved in deep layers of M2. In view of long-range intracortical  
584 connections between S1 and M2, specifically from layer V/VI of S1 to layer V of M2 (Condé  
585 et al. 1995; Zhang and Deschênes 1997; Zakiewicz et al. 2014; Reep and Corwin 1999), the  
586 high SWD prediction performance in S1 compared to M2 suggests that SWD precursor

587 activity is a locally restricted cortical phenomenon, at least with regard to the initiation zone in  
588 S1.

589 Prediction performance of the Maksimenko et al. (2017)-algorithm was found to differ  
590 between the two genetic model strains, in that prediction performance was generally more  
591 accurate and spectra corresponding to true and false positive detections were more  
592 differentiated in GAERS compared to WAG/Rij rats. Differences between the two models and  
593 even between different colonies of the same strain have been described for distinct  
594 electrographic features of the SWDs (Akman et al. 2010; Powell et al. 2014). It is likely that  
595 that the frequency band  $W_{(5-10 \text{ Hz})}$ , employed by the algorithm for precursor detection, better  
596 suits detection of 5-9 Hz oscillations, which have been described to precede SWDs in  
597 GAERS (Pinault et al. 2001). In WAG/Rij rats, on the other hand, precursor activity has been  
598 described in both theta and delta frequency bands (van Luijtelaar et al. 2016; van Luijtelaar  
599 et al. 2011), implying that improved SWD prediction performance in WAG/Rij rats might  
600 require additional fine-tuning of the frequency band width applied by the Maksimenko et al.  
601 2017 algorithm.

602

#### 603 **4.2 Random forest machine learning algorithm for the reduction of false alarms.**

604 Irrespective of the combination of recording sites, false alarm rates remained at a relatively  
605 high level. However, statistical comparison between wavelet spectra of true positive and  
606 false positive predictions were revealed to significantly differ in their wavelet energies in both  
607 strains and a random forest machine learning algorithm could be trained to detect such pre-  
608 existing spectral differences to further differentiate between true and false positive  
609 predictions. In long lasting, out-of sample, 24 hours recordings in the deep layers of S1 in  
610 nine GAERS, which cover the full diurnal variation reported for SWD occurrence (Smyk and  
611 van Luijtelaar 2020), this additional classification of a trained random forest reduced the false  
612 alarm rate for SWD prediction by an average of 71,4%

613

614 Of note, the balanced accuracy of classification depended on the approach of training (i.e.  
615 oversampling vs. undersampling) introduced to the random forest. Machine learning  
616 algorithms require a balanced training set in order for unbiased assessments of error rates to  
617 be achieved (Khan et al. 2018). With respect to SWDs, precursor and true positive  
618 predictions are an underrepresented class compared to the much larger group of interictal  
619 and false positive predictions. For balance training, random undersampling and (moderate)  
620 random oversampling (Chawla et al. 2002; Kubat et al. 1997) were used, and classification  
621 performance of two differentially trained random forests were compared. Significantly higher  
622 balanced accuracies were found for the random forest trained in the moderate oversampling  
623 approach as compared to the under-sampling approach, suggesting that undersampling

624 does not include the full spectrum of variance among different types of false positive  
625 detections.

626

627 Another common source of error in machine learning algorithms is the choice of the  
628 dataset on which algorithm performance is evaluated. As mentioned above, in line with  
629 guidelines of good scientific practice (Kuhlmann et al. 2018; Mormann et al. 2007), algorithm  
630 performance was evaluated both in unseen in-sample recordings of the same rats (30% of  
631 unseen data) as well as in lasting, non-selected, pseudo-prospective 24 hours recordings  
632 acquired in a separate group of GAERS (out-of sample evaluation). The importance of such  
633 an additional validation step can readily be inferred from the drop in algorithm performance  
634 between in-sample and out-of sample testing. Furthermore, our attempt to confront the  
635 algorithm with the full range of diurnal variations necessitated these 24 hours recordings.

636

637 Unfortunately, classification by the random forest also went along, to some degree, with a  
638 decrease in prediction sensitivity, in that 200 out of 409 SWD were correctly predicted  
639 (corresponding to a decrease in sensitivity by 41%). The prediction of SWDs thus lacks  
640 behind the performance of prediction systems aimed at focal convulsive seizures, reaching  
641 sensitivities of prediction up to around 90% (Kiral-Kornek et al. 2018; Khan et al. 2018;  
642 Kuhlmann et al. 2018). Of note, SWDs in absence epilepsy constitute a type of seizure that  
643 is fundamental different from focal convulsive seizures, in terms of pharmacological profile,  
644 frequency of occurrence, pathomechanisms, and interictal spike patterns (Depaulis and van  
645 Luijtelaar 2006). Moreover, the moderate performance of SWD prediction may relate to inter-  
646 individual differences, which are visible in both in-sample and out-of sample validation.  
647 Spatial variance between the position of the recording electrodes relative to the initiation  
648 zone in S1, or neurobiological differences in the cortical initiation network between  
649 individuals (Meeren et al. 2002) may explain these findings. As a corollary, individualized  
650 training of the random forest on long-term data obtained from a single individual may fine-  
651 tune and improve random forest approaches to SWD prediction.

652

### 653 **4.3 Possible translation to prediction of SWDs in human absence epilepsy**

654 SWD prediction performance of the Maksimenko et al (2017) and combined classification  
655 performance of the random forest was best for intracortical recordings obtained in close  
656 proximity to the seizure initiation network in S1. These findings provide an interesting  
657 perspective for SWD prediction in humans using surface EEG recordings. As in the genetic  
658 rat models, a local cortical initiation site of SWDs has been identified using EEG and MEG  
659 recordings combined with non-linear association analysis in children with absence epilepsy

660 (Westmijse et al. 2009; Ossenblok et al. 2019). Moreover, Gupta and colleagues (2011)  
661 identified pre-ictal sources of activity, occurring approximately 1 second prior to SWDs. Of  
662 note, the exact location of the cortical SWD onset zone is variable between individual  
663 children and pre-ictal activity was reported to be most pronounced in the delta frequency  
664 range. Fine tuning of the frequency bands analyzed by the Maksimenko et al algorithm, and  
665 training of the random forest on long-lasting EEG recordings in an individual child, are thus  
666 promising possibilities paving the way for SWD prediction in children.  
667 Wavelet analysis is a fast and reliable method for assessing non-stationary signals like LFP-  
668 or EEG recordings (Hramov et al. 2015). Together with the fast temporal precision of EEG  
669 and LFP recordings, this approach allows a detection of fast and short lasting events like  
670 SWD precursors and opens the door for an implementation in an on-line setting aimed at real  
671 time prediction and prevention (Maksimenko et al. 2017) with as little interference to the  
672 overall brain activity as possible (van Luijtelaar et al. 2017; Osterhagen et al. 2010). Such a  
673 treatment approach might go along with a strong relief of side-effects often reported for the  
674 commonly used chronic pharmaceutical interventions (Crunelli et al. 2020).

675

## 676 **References**

- 677 2016 Community Survey of Epilepsy Innovation Institute (Ei2) (2016). USA. Available online  
678 at [https://www.epilepsy.com/sites/core/files/atoms/files/community-survey-report-](https://www.epilepsy.com/sites/core/files/atoms/files/community-survey-report-2016%20V2.pdf)  
679 [2016%20V2.pdf](https://www.epilepsy.com/sites/core/files/atoms/files/community-survey-report-2016%20V2.pdf).
- 680 Akman, Ozlem; Demiralp, Tamer; Ates, Nurbay; Onat, Filiz Yilmaz (2010):  
681 Electroencephalographic differences between WAG/Rij and GAERS rat models of absence  
682 epilepsy. In *Epilepsy research* 89 (2), pp. 185–193. DOI: 10.1016/j.eplepsyres.2009.12.005.
- 683 Birjandtalab, Javad; Baran Pouyan, Maziyar; Cogan, Diana; Nourani, Mehrdad; Harvey, Jay  
684 (2017): Automated seizure detection using limited-channel EEG and non-linear dimension  
685 reduction. In *Computers in Biology and Medicine* 82, pp. 49–58. DOI:  
686 10.1016/j.combiomed.2017.01.011.
- 687 Chawla, N. V.; Bowyer, K. W.; Hall, L. O.; Kegelmeyer, W. P. (2002): SMOTE: Synthetic  
688 Minority Over-sampling Technique. In *jair* 16, pp. 321–357. DOI: 10.1613/jair.953.
- 689 Condé, F.; Maire-Lepoivre, E.; Audinat, E.; Crépel, F. (1995): Afferent connections of the  
690 medial frontal cortex of the rat. II. Cortical and subcortical afferents. In *The Journal of*  
691 *comparative neurology* 352 (4), pp. 567–593. DOI: 10.1002/cne.903520407.
- 692 Crunelli, Vincenzo; Lőrincz, Magor L.; McCafferty, Cian; Lambert, Régis C.; Leresche,  
693 Nathalie; Di Giovanni, Giuseppe; David, François (2020): Clinical and experimental insight  
694 into pathophysiology, comorbidity and therapy of absence seizures. In *Brain* 143 (8),  
695 pp. 2341–2368. DOI: 10.1093/brain/awaa072.

- 696 Daily, Mike; Medasani, Swarup; Behringer, Reinhold; Trivedi, Mohan (2017): Self-Driving  
697 Cars. In *Computer* 50 (12), pp. 18–23. DOI: 10.1109/MC.2017.4451204.
- 698 Depaulis, Antoine; Charpier, Stéphane (2018): Pathophysiology of absence epilepsy:  
699 Insights from genetic models. In *Neuroscience letters* 667, pp. 53–65. DOI:  
700 10.1016/j.neulet.2017.02.035.
- 701 Depaulis, Antoine; David, Olivier; Charpier, Stéphane (2016): The genetic absence epilepsy  
702 rat from Strasbourg as a model to decipher the neuronal and network mechanisms of  
703 generalized idiopathic epilepsies. In *Journal of neuroscience methods* 260, pp. 159–174.  
704 DOI: 10.1016/j.jneumeth.2015.05.022.
- 705 Depaulis, Antoine; van Luijckelaar, Gilles (2006): Genetic models of absence epilepsy. In  
706 Pitkanen, A., Schwartzkroin, P.P., Moshe, S.L. (Ed.): *Models of Seizures and Epilepsy*.  
707 SanDiego: Elsevier Academic Press.
- 708 Depauls, A.; Vergnes, M.; Liu, Z.; Kempf, E.; Marescaux, C. (1990): Involvement of the nigral  
709 output pathways in the inhibitory control of the substantia nigra over generalized non-  
710 convulsive seizures in the rat. In *Neuroscience* 39 (2), pp. 339–349. DOI: 10.1016/0306-  
711 4522(90)90272-6.
- 712 Eberlein, Matthias; Müller, Jens; Yang, Hongliu; Walz, Simon; Schreiber, Janina; Tetzlaff,  
713 Ronald et al. (2019): Evaluation of machine learning methods for seizure prediction in  
714 epilepsy. In *Current Directions in Biomedical Engineering* 5 (1), pp. 109–112. DOI:  
715 10.1515/cdbme-2019-0028.
- 716 Gupta, Disha; Ossenblok, Pauly; van Luijckelaar, Gilles (2011): Space-time network  
717 connectivity and cortical activations preceding spike wave discharges in human absence  
718 epilepsy: a MEG study. In *Medical & biological engineering & computing* 49 (5), pp. 555–565.  
719 DOI: 10.1007/s11517-011-0778-3.
- 720 Hramov, Alexander E.; Koronovskii, Alexey A.; Makarov, Valeri A.; Pavlov, Alexey N.;  
721 Sitnikova, Evgenia (2015): *Wavelets in Neuroscience*. Heidelberg: Springer (Springer Series  
722 in Synergetics). Available online at <http://gbv.ebib.com/patron/FullRecord.aspx?p=1802957>.
- 723 Jarre, Guillaume; Altwegg-Boussac, Tristan; Williams, Mark S.; Studer, Florian; Chipaux,  
724 Mathilde; David, Olivier et al. (2017): Building Up Absence Seizures in the Somatosensory  
725 Cortex: From Network to Cellular Epileptogenic Processes. In *Cerebral cortex (New York,*  
726 *N.Y. : 1991)* 27 (9), pp. 4607–4623. DOI: 10.1093/cercor/bhx174.
- 727 Khan, Haidar; Marcuse, Lara; Fields, Madeline; Swann, Kalina; Yener, Bulent (2018): Focal  
728 Onset Seizure Prediction Using Convolutional Networks. In *IEEE transactions on bio-medical*  
729 *engineering* 65 (9), pp. 2109–2118. DOI: 10.1109/TBME.2017.2785401.
- 730 Kiral-Kornek, Isabell; Roy, Subhrajit; Nurse, Ewan; Mashford, Benjamin; Karoly, Philippa;  
731 Carroll, Thomas et al. (2018): Epileptic Seizure Prediction Using Big Data and Deep  
732 Learning: Toward a Mobile System. In *EBioMedicine* 27, pp. 103–111. DOI:  
733 10.1016/j.ebiom.2017.11.032.
- 734 Kubat, Miroslav; Holte, Robert; Matwin, Stan (1997): Learning when negative examples  
735 abound. In Maarten Someren, Gerhard Widmer (Eds.): *Machine Learning: ECML-97*. 9th

- 736 European Conference on Machine Learning Prague, Czech Republic, April 23-25, 1997  
737 Proceedings, vol. 1224. Berlin, Heidelberg: Springer (Lecture Notes in Computer Science,  
738 Lecture Notes in Artificial Intelligence, 1224), pp. 146–153.
- 739 Kuhlmann, Levin; Lehnertz, Klaus; Richardson, Mark P.; Schelter, Björn; Zaveri, Hitten P.  
740 (2018): Seizure prediction - ready for a new era. In *Nature reviews. Neurology* 14 (10),  
741 pp. 618–630. DOI: 10.1038/s41582-018-0055-2.
- 742 Lopes Da Silva; Blanes; Kalitzin; Parra; Suffczynski; Velis (2003): Epilepsies as Dynamical  
743 Diseases of Brain Systems: Basic Models of the Transition Between Normal and Epileptic  
744 Activity. In *Epilepsia* 44, pp. 72–83. DOI: 10.1111/j.0013-9580.2003.12005.x.
- 745 Lüttjohann, Annika; Pape, Hans-Christian (2019): Regional specificity of cortico-thalamic  
746 coupling strength and directionality during waxing and waning of spike and wave discharges.  
747 In *Scientific reports* 9 (1), p. 2100. DOI: 10.1038/s41598-018-37985-7.
- 748 Lüttjohann, Annika; van Luijteleaar, Gilles (2012): The dynamics of cortico-thalamo-cortical  
749 interactions at the transition from pre-ictal to ictal LFPs in absence epilepsy. In *Neurobiology*  
750 *of disease* 47 (1), pp. 49–60. DOI: 10.1016/j.nbd.2012.03.023.
- 751 Lüttjohann, Annika; van Luijteleaar, Gilles (2015): Dynamics of networks during absence  
752 seizure's on- and offset in rodents and man. In *Front. Physiol.* 6, p. 16. DOI:  
753 10.3389/fphys.2015.00016.
- 754 Maksimenko, Vladimir A.; van Heukelum, Sabrina; Makarov, Vladimir V.; Kelderhuis, Janita;  
755 Lüttjohann, Annika; Koronovskii, Alexey A. et al. (2017): Absence Seizure Control by a Brain  
756 Computer Interface. In *Scientific reports* 7 (1), p. 2487. DOI: 10.1038/s41598-017-02626-y.
- 757 Meeren, Hanneke K. M.; Pijn, Jan Pieter M.; van Luijteleaar, Egidius L. J. M.; Coenen, Anton  
758 M. L.; Lopes da Silva, Fernando H. (2002): Cortical Focus Drives Widespread  
759 Corticothalamic Networks during Spontaneous Absence Seizures in Rats. In *J. Neurosci.* 22  
760 (4), pp. 1480–1495. DOI: 10.1523/JNEUROSCI.22-04-01480.2002.
- 761 Mormann, Florian; Andrzejak, Ralph G.; Elger, Christian E.; Lehnertz, Klaus (2007): Seizure  
762 prediction: the long and winding road. In *Brain* 130 (2), pp. 314–333. DOI:  
763 10.1093/brain/awl241.
- 764 Ossenblok, Pauly; van Houdt, Petra; Colon, Albert; Stroink, Hans; van Luijteleaar, Gilles  
765 (2019): A network approach to investigate the bi-hemispheric synchrony in absence epilepsy.  
766 In *Clinical neurophysiology : official journal of the International Federation of Clinical*  
767 *Neurophysiology* 130 (9), pp. 1611–1619. DOI: 10.1016/j.clinph.2019.05.034.
- 768 Osterhagen, Lasse; Breteler, Marinus; van Luijteleaar, Gilles (2010): Does arousal interfere  
769 with operant conditioning of spike-wave discharges in genetic epileptic rats? In *Epilepsy*  
770 *research* 90 (1), pp. 75–82. DOI: 10.1016/j.eplepsyres.2010.03.010.
- 771 Panayiotopoulos, C. P.; Chroni, E.; Daskalopoulos, C.; Baker, A.; Rowlinson, S.; Walsh, P.  
772 (1992): Typical absence seizures in adults: clinical, EEG, video-EEG findings and  
773 diagnostic/syndromic considerations. In *Journal of neurology, neurosurgery, and psychiatry*  
774 55 (11), pp. 1002–1008. DOI: 10.1136/jnnp.55.11.1002.

- 775 Paxinos, G. Watson C. (1998): The Rat Brain in Stereotactic Coordinates. London: Academic  
776 Press, Ltd.
- 777 Pinault, D.; Vergnes, M.; Marescaux, C. (2001): Medium-voltage 5-9-Hz oscillations give rise  
778 to spike-and-wave discharges in a genetic model of absence epilepsy: in vivo dual  
779 extracellular recording of thalamic relay and reticular neurons. In *Neuroscience* 105 (1),  
780 pp. 181–201. DOI: 10.1016/s0306-4522(01)00182-8.
- 781 Polack, Pierre-Olivier; Guillemain, Isabelle; Hu, Emilie; Deransart, Colin; Depaulis, Antoine;  
782 Charpier, Stéphane (2007): Deep layer somatosensory cortical neurons initiate spike-and-  
783 wave discharges in a genetic model of absence seizures. In *The Journal of neuroscience :*  
784 *the official journal of the Society for Neuroscience* 27 (24), pp. 6590–6599. DOI:  
785 10.1523/JNEUROSCI.0753-07.2007.
- 786 Powell, Kim L.; Tang, Howard; Ng, Caroline; Guillemain, Isabelle; Dieuset, Gabriel; Dezsi,  
787 Gabi et al. (2014): Seizure expression, behavior, and brain morphology differences in  
788 colonies of Genetic Absence Epilepsy Rats from Strasbourg. In *Epilepsia* 55 (12), pp. 1959–  
789 1968. DOI: 10.1111/epi.12840.
- 790 Ratner, Mark (2015): IBM's Watson Group signs up genomics partners. In *Nature*  
791 *biotechnology* 33 (1), pp. 10–11. DOI: 10.1038/nbt0115-10.
- 792 Reep, R. L.; Corwin, J. V. (1999): Topographic organization of the striatal and thalamic  
793 connections of rat medial agranular cortex. In *Brain research* 841 (1-2), pp. 43–52. DOI:  
794 10.1016/s0006-8993(99)01779-5.
- 795 Seizure Gauge Challenge (2017). Edited by Epilepsy Foundation. USA. Available online at  
796 [https://www.epilepsy.com/about-us/research-and-new-therapies/innovation/epilepsy-](https://www.epilepsy.com/about-us/research-and-new-therapies/innovation/epilepsy-innovation-institute/seizure-gauge-challenge)  
797 [innovation-institute/seizure-gauge-challenge.](https://www.epilepsy.com/about-us/research-and-new-therapies/innovation/epilepsy-innovation-institute/seizure-gauge-challenge)
- 798 Sitnikova, Evgenia; Hramov, Alexander E.; Koronovsky, Alexey A.; van Luijtelaar, Gilles  
799 (2009): Sleep spindles and spike-wave discharges in EEG: Their generic features,  
800 similarities and distinctions disclosed with Fourier transform and continuous wavelet analysis.  
801 In *Journal of neuroscience methods* 180 (2), pp. 304–316. DOI:  
802 10.1016/j.jneumeth.2009.04.006.
- 803 Sitnikova, Evgenia; van Luijtelaar, Gilles (2007): Electroencephalographic Characterization of  
804 Spike-Wave Discharges in Cortex and Thalamus in WAG/Rij Rats. In *Epilepsia* 0 (0),  
805 070810012536001-??? DOI: 10.1111/j.1528-1167.2007.01250.x.
- 806 Smyk, Magdalena K.; van Luijtelaar, Gilles (2020): Circadian Rhythms and Epilepsy: A  
807 Suitable Case for Absence Epilepsy. In *Frontiers in neurology* 11, p. 245. DOI:  
808 10.3389/fneur.2020.00245.
- 809 Sorokin, Jordan M.; Paz, Jeanne T.; Huguenard, John R. (2016): Absence seizure  
810 susceptibility correlates with pre-ictal  $\beta$  oscillations. In *Journal of physiology, Paris* 110 (4 Pt  
811 A), pp. 372–381. DOI: 10.1016/j.jphysparis.2017.05.004.
- 812 van Luijtelaar, G.; Zobeiri, M. (2014): Progress and outlooks in a genetic absence epilepsy  
813 model (WAG/Rij). In *Current medicinal chemistry* 21 (6), pp. 704–721. DOI:  
814 10.2174/0929867320666131119152913.

815 van Luijtelaar, G. V.; Zobeiri, M.; Lüttjohann, A.; Depaulis, A. (2017): Experimental Treatment  
816 Options in Absence Epilepsy. In *Current pharmaceutical design* 23 (37). DOI:  
817 10.2174/1381612823666171017170226.

818 van Luijtelaar, Gilles; Hramov, Alexander; Sitnikova, Evgenia; Koronovskii, Alexei (2011):  
819 Spike-wave discharges in WAG/Rij rats are preceded by delta and theta precursor activity in  
820 cortex and thalamus. In *Clinical neurophysiology : official journal of the International*  
821 *Federation of Clinical Neurophysiology* 122 (4), pp. 687–695. DOI:  
822 10.1016/j.clinph.2010.10.038.

823 van Luijtelaar, Gilles; Lüttjohann, Annika; Makarov, Vladimir V.; Maksimenko, Vladimir A.;  
824 Koronovskii, Alexei A.; Hramov, Alexander E. (2016): Methods of automated absence  
825 seizure detection, interference by stimulation, and possibilities for prediction in genetic  
826 absence models. In *Journal of neuroscience methods* 260, pp. 144–158. DOI:  
827 10.1016/j.jneumeth.2015.07.010.

828 Walter, Martin; Alizadeh, Sarah; Jamalabadi, Hamidreza; Lueken, Ulrike; Dannlowski, Udo;  
829 Walter, Henrik et al. (2019): Translational machine learning for psychiatric neuroimaging. In  
830 *Progress in neuro-psychopharmacology & biological psychiatry* 91, pp. 113–121. DOI:  
831 10.1016/j.pnpbp.2018.09.014.

832 Westmijse, Inge; Ossenblok, Pauly; Gunning, Boudewijn; van Luijtelaar, Gilles (2009): Onset  
833 and propagation of spike and slow wave discharges in human absence epilepsy: A MEG  
834 study. In *Epilepsia* 50 (12), pp. 2538–2548. DOI: 10.1111/j.1528-1167.2009.02162.x.

835 Zakiewicz, Izabela M.; Bjaalie, Jan G.; Leergaard, Trygve B. (2014): Brain-wide map of  
836 efferent projections from rat barrel cortex. In *Frontiers in neuroinformatics* 8, p. 5. DOI:  
837 10.3389/fninf.2014.00005.

838 Zhang, Z. W.; Deschênes, M. (1997): Intracortical axonal projections of lamina VI cells of the  
839 primary somatosensory cortex in the rat: a single-cell labeling study. In *The Journal of*  
840 *neuroscience : the official journal of the Society for Neuroscience* 17 (16), pp. 6365–6379.

841

842

843

844

845

846

847

848

849

850

851

852

853

854

855 **Figure legends and tables**

856 **Figure 1:** Exemplary local field potential recordings in the deep somatosensory cortex of a  
857 GAERS (right) as well as simultaneously recorded LFPs the deep somatosensory cortex and  
858 vertral-postero-medial thalamic nucleus (VPM) of a WAG/Rij rat (upper left panel and lower  
859 left panel, respectively). Arrows indicates the onset of the SWD, determined according to the  
860 criteria outlined by van Luijtelaar & Coenen (1986), taking the peak of the first spike of twice  
861 the background as reference for SWD onset.

862

863 **Figure 2:** Wavelet analysis for SWD prediction. Relative sensitivity (A) and average false  
864 alarm rate (C) of SWD prediction for different combinations of recording sites in the cortico-  
865 thalamic system, obtained by the Maksimenko et al. (2017) algorithm. LFPs, simultaneously  
866 recorded in the cortico-thalamic system of WAG-Rij rats (see methods), were analyzed in  
867 combinations of either two or three recording sites. Results from all 85 combinations are  
868 presented in Table I. To avoid type II errors, all combinations of recording sites were grouped  
869 as either 'CC' (two intracortical recording sites in S1), 'CT' (one cortical recording site in S1  
870 and one thalamic recording site), 'TT' (two intrathalamic recording sites, 'CCC' (three  
871 intracortical recording sites in S1), 'CCT' (two cortical recording sites in S1 and one thalamic  
872 recording site), 'CTT' (one cortical recording site in S1 and two thalamic recording sites),  
873 'TTT' (three intrathalamic recording sites) or 'MCCC' (three intracortical recording sites in the  
874 secondary motor cortex), respectively. B, C: Results of post-hoc comparison verified by  
875 ANOVA, with \*\*\* indicating significance at a  $p < 0.001$  level for sensitivity of prediction (B) and  
876 false alarm rate (D), respectively. E: Relationship of false alarm rates and average sensitivity  
877 of SWD prediction for different combinations of recording sites in the cortico-thalamic system  
878 of WAG/Rij rats, analyzed by the Maksimenko et al. (2017) algorithm. Note highest sensitivity  
879 with a low false alarm rate for prediction based on three intracortical recordings in S1 (blue  
880 triangle) that outperforms all other combinations of recording sites. Further note the negative  
881 correlation between both indicators of SWD prediction performance ( $r = -0.716$ ;  $p < 0.001$ ),  
882 indicating that higher SWD prediction sensitivity at any given combination of recording sites  
883 does not occur at the trade-off of a high false alarm rate.

884

885 **Figure 3:** SWD prediction in two genetic rat models of absence epilepsy. A, B: Average  
886 sensitivity of SWD prediction (A) and false alarm rate expressed in number false positives  
887 per hour (nFP/h) (B) achieved by the Maksimenko et al. (2017) algorithm assessed in 4  
888 hours lasting LFP recordings, obtained in layers IV, V and VI of S1 in GAERS and WAG/Rij  
889 rats.

890 C - E: Comparison of wavelet spectra of true and false positive predictions. An exemplary  
891 LFP trace depicting a pre-SWD → SWD transition is presented in (C). Onset of SWD is  
892 marked by red vertical line termed 2. The corresponding spectrogram of a true positive  
893 detection identified in intracortical LFP recordings in S1 of a GAERS is shown in (D). Time  
894 point -0.5 to 0 (red rectangle termed 1) features the analysis window (window size 500 ms) in  
895 which the true positive precursor is detected. An exemplary spectrogram of a false positive  
896 detection is shown in (E). Again, time point -0.5 to 0 features the analysis window (window  
897 size 500 ms) in which the false positive precursor is detected. F: Statistical comparison of the  
898 product of wavelet energy, assessed in the frequency bands  $W_{(5-10 \text{ Hz})}$ ,  $W_{(3-5 \text{ Hz})}$  and  $W_{(7-20 \text{ Hz})}$   
899 (Maksimenko et al. 2017), between true and false positives in WAG/Rij rats. E: Statistical  
900 comparison of the product of wavelet energy, assessed in the frequency bands  $W_{(5-10 \text{ Hz})}$ ,  $W_{(3-5 \text{ Hz})}$   
901 and  $W_{(7-20 \text{ Hz})}$  (Maksimenko et al. 2017), between true and false positives in GAERS. \*\*\*  
902 indicates a significant difference verified by ANOVA at level of  $p < 0.001$ ; \*\* at a level of  
903  $p < 0.01$ ; and \* at level of  $p < 0.05$ .

904

905 **Figure 4:** Differentiation between true- and false positives by a random forest machine  
906 learning algorithm. A: Schematic representation of the random forest machine learning  
907 algorithm for differentiation between true positive and false positive predictions. After wavelet  
908 analysis of either two or three simultaneously recorded LFP traces, the wavelet energies  
909 ( $W_{(5-10 \text{ Hz})}$ ,  $W_{(3-5 \text{ Hz})}$  and  $W_{(7-20 \text{ Hz})}$ ) extracted in each trace are fed to a random forest composed  
910 of 1000 decision trees. Final classification of the random forest is yielded from a majority  
911 voting of the different trees (see methods for detail). B: Out-of-sample performance  
912 (expressed as balanced accuracy) of random forests. Training in an undersampling  
913 approach on wavelet spectra derived from recordings in layers V and VI of S1 (CC),  
914 recordings in layers IV, V and VI of S1 (CCC), recordings in layers IV, VI of S1 and VPM  
915 (CCT), recordings in layer VI of S1, VPM and RTN (CTT), recordings in VPM, cRTN and Po  
916 (TTT) of WAG/Rij rats at a sensitivity of 60%, and recordings in layers IV, V and VI of S1 of  
917 GAERS at a sensitivity of 60% (GCCC) or 90% (GCCC90%). Numbers in GAERS groups  
918 (1844, 161, 145) refer to the different amount of true/false positive fragments, with which the  
919 random forest was trained. Stars in B indicate a significant classification above chance as  
920 validated by surrogate statistics with \* indicating significance at a  $p < 0.05$ , \*\*  $p < 0.01$  and \*\*\*

921  $p < 0.001$  level. C: Table of achieved average balanced accuracies achieved by analysis of  
 922 the different combinations of recording sites. D: Statistics between group comparison of  
 923 balanced accuracies performed with ANOVA with \* indicating significance at a  $p < 0.05$ , \*\*  
 924  $p < 0.01$  and \*\*\*  $p < 0.001$  level. E: Relation between classification accuracy and the number of  
 925 incorporated trees in the random forest.

926 **Table I: Combinations of recording sites analyzed by the Maksimenko et al. algorithm and**  
 927 **achieved average sensitivities of prediction and false alarm rates.** Abbreviations: ctx4: layer 4 of  
 928 somatosensory cortex, ctx5: layer 5 of somatosensory cortex, ctx6: layer 6 of somatosensory cortex,  
 929 ATN: anterior thalamic nucleus, VPM: vertral-postero-medial thalamic nucleus, PO: posterior thalamic  
 930 nucleus, rRTN: rostral reticular thalamic nucleus, cRTN: caudal reticular thalamic nucleus, Mctx5a:  
 931 layer 5a of secondary motor cortex, Mctx5b: layer 5b of secondary motor cortex, Mctx6: layer 6 of  
 932 secondary motor cortex

number of simultaneous recording sites	combination number	area 1	area 1	area 3	abbreviation in text and figures	average sensitivity	average nFP/h
3	1	ctx 4	ctx 5	ctx 6	CCC	61,755	85,962
	2	ctx 4	ctx 5	Po	CCT	48,392	65,199
	3	ctx 4	ctx 5	ATN	CCT	45,974	85,363
	4	ctx 4	ctx 5	rRTN	CCT	44,230	69,947
	5	ctx 4	ctx 5	cRTN	CCT	50,600	58,431
	6	ctx 4	ctx 5	VPM	CCT	46,007	61,826
	7	ctx 4	ctx 6	Po	CCT	50,718	68,470
	8	ctx 4	ctx 6	ATN	CCT	48,932	82,776
	9	ctx 4	ctx 6	rRTN	CCT	45,690	71,436
	10	ctx 4	ctx 6	cRTN	CCT	51,823	60,125
	11	ctx 4	ctx 6	VPM	CCT	50,269	58,889
	12	ctx 5	ctx 6	Po	CCT	48,880	79,424
	13	ctx 5	ctx 6	ATN	CCT	48,345	95,587
	14	ctx 5	ctx 6	rRTN	CCT	51,354	65,995
	15	ctx 5	ctx 6	cRTN	CCT	48,963	72,081
	16	ctx 5	ctx 6	VPM	CCT	48,708	62,217
	17	ctx 4	Po	ATN	CTT	36,121	98,180
	18	ctx 4	Po	rRTN	CTT	35,171	97,276
	19	ctx 4	Po	cRTN	CTT	35,430	95,410
	20	ctx 4	Po	VPM	CTT	34,470	99,526

21	ctx 4	ATN	rRTN	CTT	38,536	82,294
22	ctx 4	ATN	cRTN	CTT	34,133	101,225
23	ctx 4	ATN	VPM	CTT	32,981	99,376
24	ctx 4	rRTN	cRTN	CTT	35,892	93,150
25	ctx 4	rRTN	VPM	CTT	33,018	101,039
26	ctx 4	cRTN	VPM	CTT	37,588	83,424
27	ctx 5	Po	ATN	CTT	38,046	96,665
28	ctx 5	Po	rRTN	CTT	36,549	93,522
29	ctx 5	Po	cRTN	CTT	36,114	97,002
30	ctx 5	Po	VPM	CTT	34,702	99,814
31	ctx 5	ATN	rRTN	CTT	40,655	77,191
32	ctx 5	ATN	cRTN	CTT	36,485	98,925
33	ctx 5	ATN	VPM	CTT	33,716	98,891
34	ctx 5	rRTN	cRTN	CTT	37,172	90,429
35	ctx 5	rRTN	VPM	CTT	33,526	100,798
36	ctx 5	cRTN	VPM	CTT	38,023	82,687
37	ctx 6	Po	ATN	CTT	40,751	95,255
38	ctx 6	Po	rRTN	CTT	38,563	93,038
39	ctx 6	Po	cRTN	CTT	38,292	95,827
40	ctx 6	Po	VPM	CTT	36,516	101,606
41	ctx 6	ATN	rRTN	CTT	43,434	72,403
42	ctx 6	ATN	cRTN	CTT	37,946	100,546
43	ctx 6	ATN	VPM	CTT	35,950	98,257
44	ctx 6	rRTN	cRTN	CTT	40,527	84,918
45	ctx 6	rRTN	VPM	CTT	35,363	100,356
46	ctx 6	cRTN	VPM	CTT	38,784	87,363
47	Po	ATN	rRTN	TTT	35,880	103,088
48	Po	ATN	cRTN	TTT	31,342	115,496
49	Po	ATN	VPM	TTT	30,849	115,094
50	Po	rRTN	cRTN	TTT	33,263	109,348
51	Po	rRTN	VPM	TTT	31,252	116,632
52	Po	cRTN	VPM	TTT	30,485	116,111

	53	ATN	rRTN	cRTN	TTT	36,646	89,893
	54	ATN	rRTN	VPM	TTT	34,497	98,061
	55	ATN	cRTN	VPM	TTT	30,137	110,576
	56	rRTN	cRTN	VPM	TTT	30,907	115,390
	57	Mctx 5a	Mctx 5b	Mctx 6	MCCC	33,330	129,803
2	1	ctx 4	ctx 5		CC	31,173	211,365
	2	ctx 4	ctx 6		CC	34,619	209,386
	3	ctx 5	ctx 6		CC	33,612	242,989
	4	ctx 4	VPM		CT	21,408	123,705
	5	ctx 4	ATN		CT	20,799	148,887
	6	ctx 4	Po		CT	21,987	151,854
	7	ctx 4	cRTN		CT	23,729	122,750
	8	ctx 4	rRTN		CT	25,276	130,967
	9	ctx 5	VPM		CT	23,357	120,332
	10	ctx 5	ATN		CT	22,728	158,520
	11	ctx 5	Po		CT	24,474	151,471
	12	ctx 5	cRTN		CT	24,874	130,418
	13	ctx 5	rRTN		CT	29,267	121,645
	14	ctx 6	VPM		CT	23,514	146,704
	15	ctx 6	ATN		CT	24,906	174,084
	16	ctx 6	Po		CT	25,886	171,314
	17	ctx 6	cRTN		CT	25,948	145,599
	18	ctx 6	rRTN		CT	31,349	137,519
	19	VPM	ATN		TT	10,411	157,414
	20	VPM	Po		TT	10,741	186,945
	21	VPM	cRTN		TT	14,999	151,043
	22	VPM	rRTN		TT	15,703	155,311
	23	ATN	Po		TT	12,648	179,928
	24	ATN	cRTN		TT	10,670	165,252
	25	ATN	rRTN		TT	20,339	142,317
	26	Po	cRTN		TT	11,267	171,176

27	Po	rRTN	TT	17,575	166,227
28	cRTN	rRTN	TT	21,339	142,157

933  
934  
935  
936  
937  
938  
939  
940  
941  
942  
943  
944  
945  
946  
947  
948  
949

Table II: Out-of-sample performance of the random forest (trained in an undersampling approach on spectra derived from three intracortical recordings in S1 of GAERS at a sensitivity of 90%) confronted to spectra derived from 24 hours recordings in a separate group of GAERS (n=9). Depicted in the upper panel is the average confusion matrix (+/- SEM), specifying the percentage of true positives correctly classified as true positives (lower right corner), true positives incorrectly classified as false positives (lower left corner), false positives correctly classified as false positives (upper left corner) and false positives incorrectly classified as true positives (upper right corner). Lower panel depicts the balanced accuracies and F1-scores for each individual rat. Note that the F1 score reflects the tradeoff between false alarm rate/sensitivity. Low F1 scores are reflecting the drop of sensitivity associated to the drop of false alarm rate. As our goal in this work is the latter, the low scores are justified by the high balanced accuracies. \* denotes an above chance balanced accuracy of classification as verified by surrogate statistics.

average confusion matrix		
predicted as false positive	52.46 % +/- 9.38	47.54 % +/- 9.38
predicted as true positive	50.66 % +/- 8.95	49.34 % +/- 8.95

	balanced accuracy	F1-score
rat 1	47,37%	14,53%
rat 2	53,68%	6,89%
rat 3	47,44%	11,74%
rat 4	49,07%	4,82%
rat 5	59,62% *	9,14%
rat 6	51,06%	5,44%
rat 7	51,93%	7,18%
rat 8	50,13%	4,25%
rat 9	47,82%	9,68%

950  
951  
952  
953  
954  
955  
956  
957

958

959

960

961

962

963 Table III: Out-of-sample performance of the random forest (trained in an oversampling approach on  
 964 spectra derived from three intracortical recordings in S1 of GAERS at a sensitivity of 90%) confronted  
 965 to spectra derived from 24 hours recordings in a separate group of GAERS (n=9).

966 Depicted in the upper panel is the average confusion matrix (+/- SEM), specifying the percentage of  
 967 true positives correctly classified as true positives (lower right corner), true positives incorrectly  
 968 classified as false positives (lower left corner), false positives correctly classified as false positives  
 969 (upper left corner) and false positives incorrectly classified as true positives (upper right corner).

970 Lower panel depicts the balanced accuracies and F1-scores for each individual rat. Note that the F1  
 971 score reflects the tradeoff between false alarm rate/sensitivity. Low F1 scores are reflecting the drop of  
 972 sensitivity associated to the drop of false alarm rate. As our goal in this work is the latter, the low  
 973 scores are justified by the high balanced accuracies. \* denotes an above chance balanced accuracy of  
 974 classification as verified by surrogate statistics.

975

976

average confusion matrix		
	predicted as false positive	predicted as true positive
false positive	71.38 % +/- 2.56	28.62 % +/- 2.56
true positive	46.00 % +/- 4.00	54.00 % +/- 4.00

	balanced accuracy	F1-score
rat 1	70,28% *	46,88%
rat 2	55,14%	7,59%
rat 3	60,13% *	16,60%
rat 4	63,98% *	12,21%
rat 5	63,15% *	12,02%
rat 6	59,70% *	8,64%
rat 7	68,47% *	13,14%
rat 8	59,00%*	6,51%
rat 9	64,38% *	19,71%

977

978

979

980

981

982

983

984

985

986

987

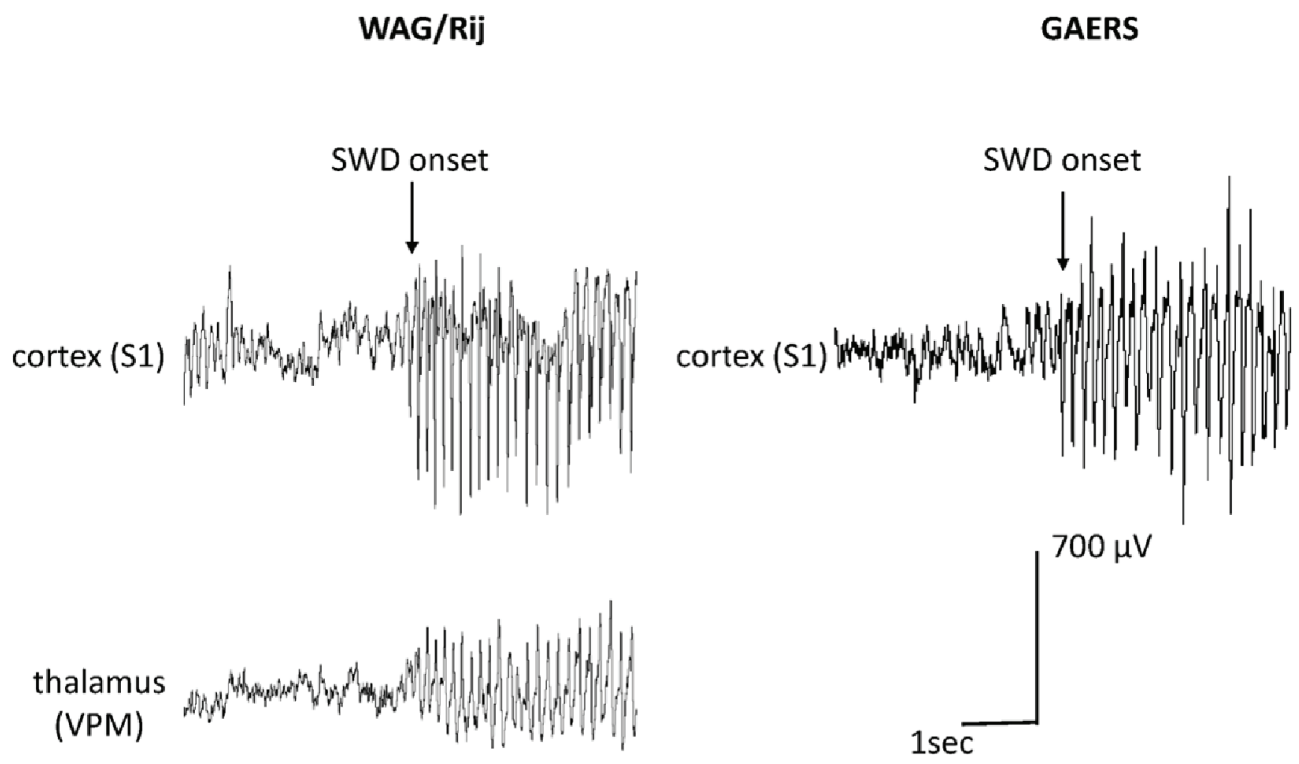
988

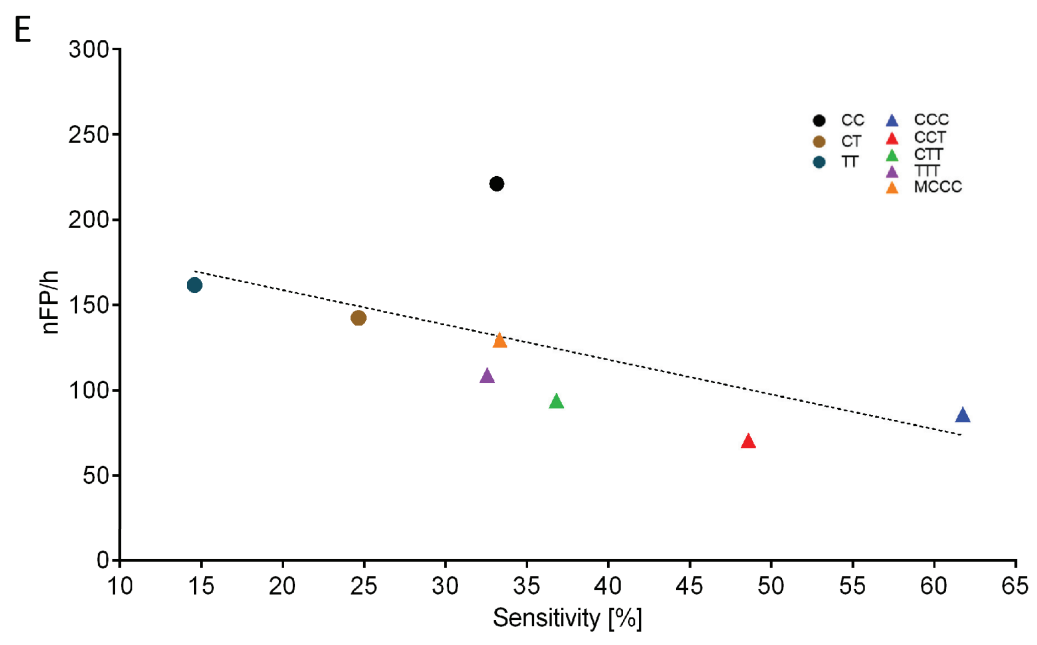
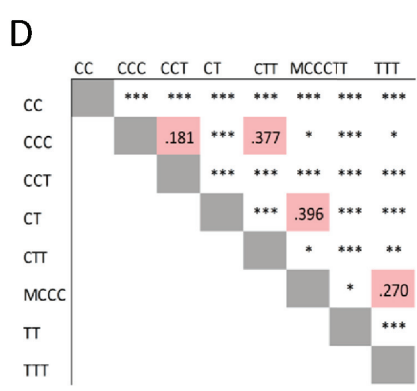
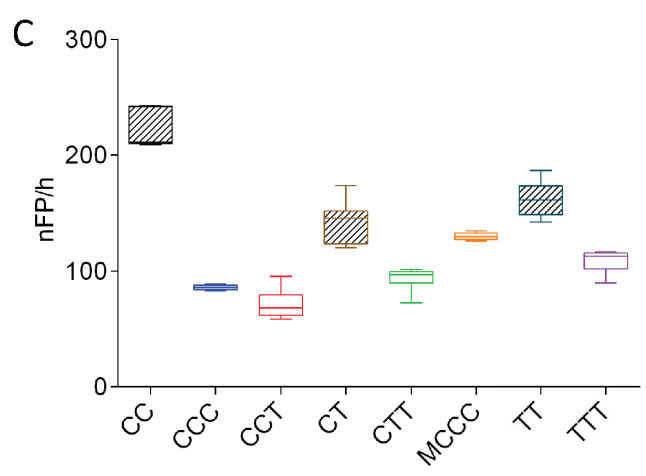
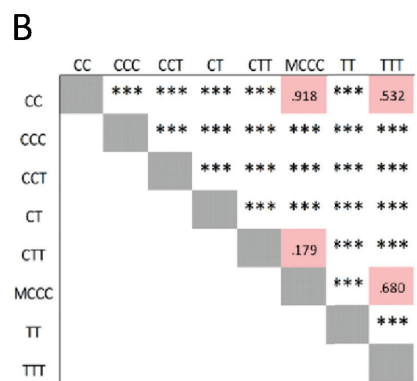
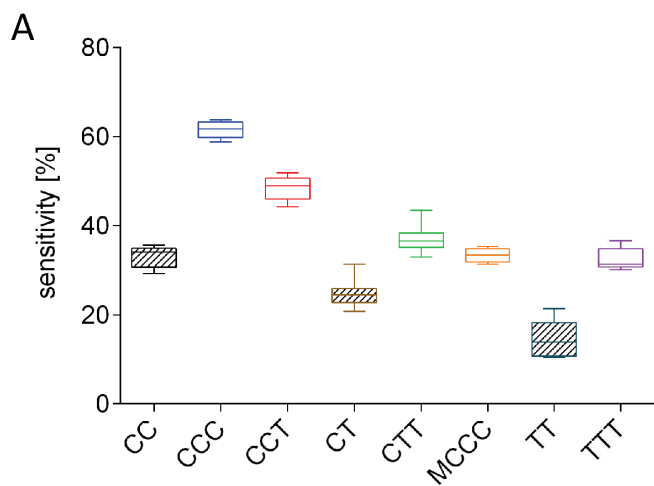
989

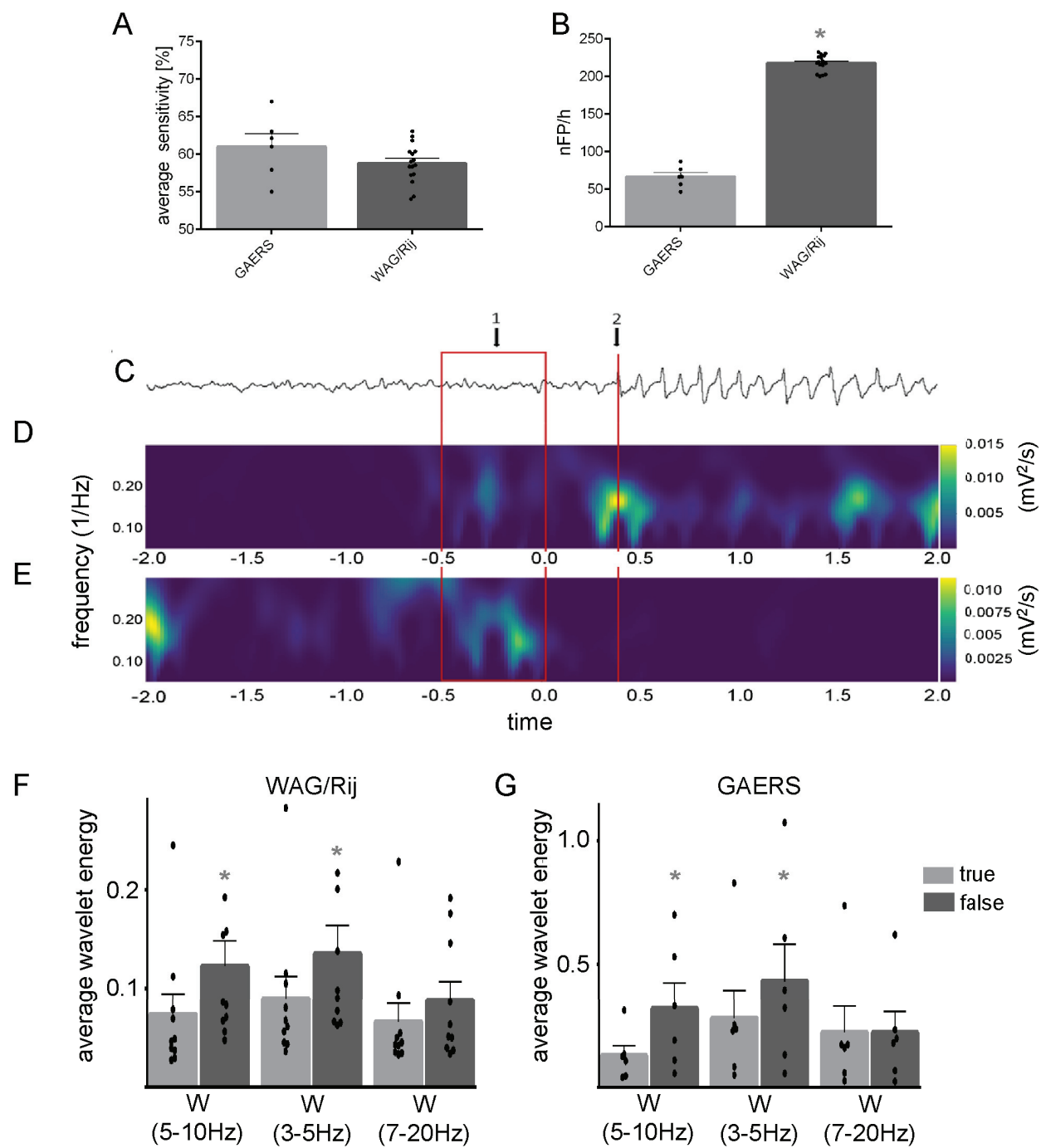
990

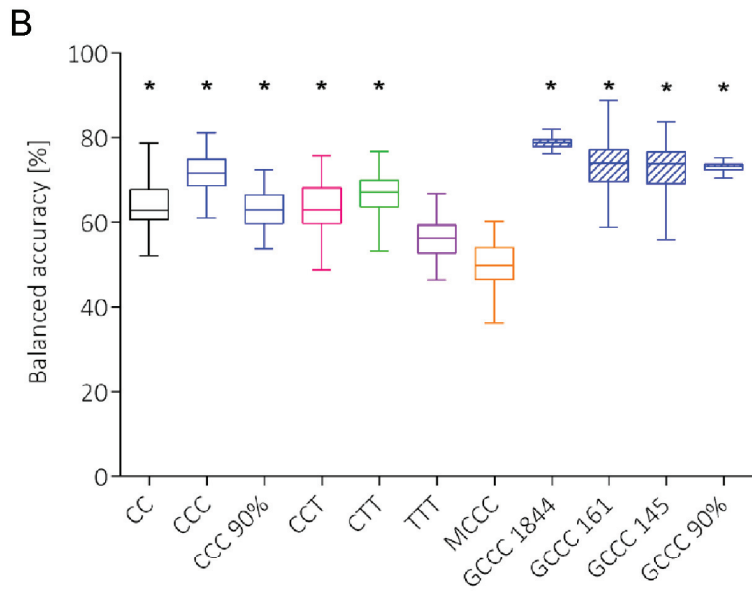
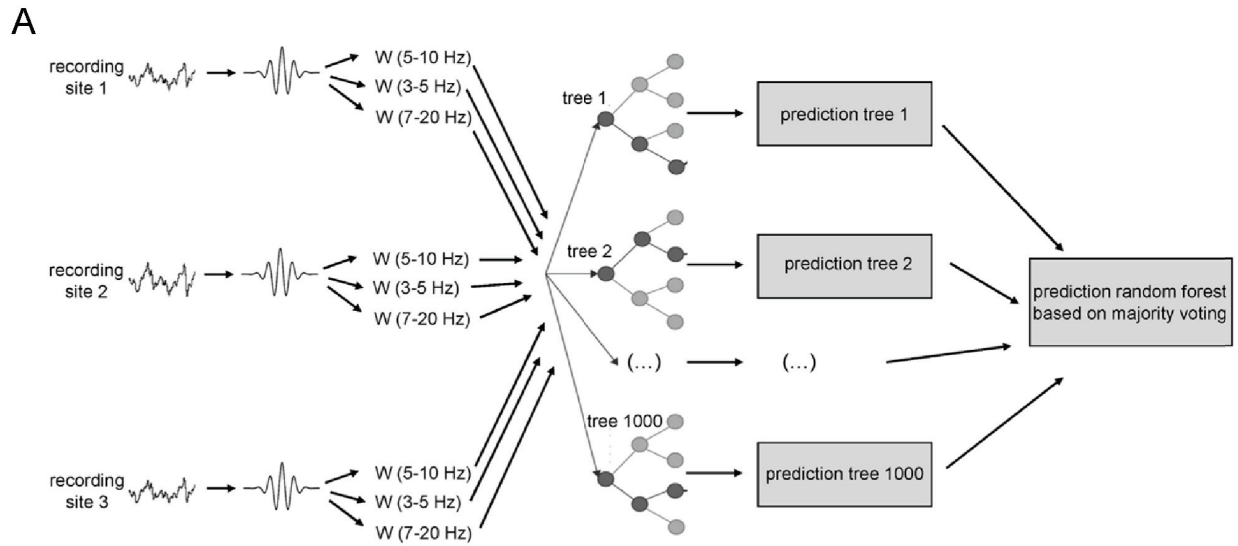
991

992









**C**

combination	balanced accuracy
CC	62.50%
CCC	71.47%
CCC 90%	63.30%
CCT	66.70%
CTT	63.20%
TTT	56.20%
MCCC	49.94%
GCCC 1841	78.80%
GCCC 161	73.58%
GCCC 145	73.00%
GCCC 90%	73.10%

